Identification and experimental validation of PYCARD as a crucial PANoptosis- related gene for immune response and inflammation in COPD

Rui Shi
Kunming Medical University
Renwen Liang
Chinese Academy of Sciences
Fang Wang
The First Affiliated Hospital of Kunming Medical University
Lueli Wang
Kunming Medical University
Wuyi Zidai
Kunming Medical University
Jie Zhang
Kunming Medical University
Luo Min
Kunming Medical University
Xiaohua Du
First Affiliated Hospital of Kunming Medical University
Shibo Sun
Kunming Medical University
Chuang Xiao
Kunming Medical University
Chaozhong Li
The First Affiliated Hospital of Kunming Medical University
Xuewu Liang
Chinese Academy of Sciences
Alex F. Chen
Shanghai Jiaotong University School of Medicine
Weimin Yang
yangweimin@kmmu.edu.cn

Kunming Medical University

Research Article

Keywords: COPD, PANoptosis, PYCARD, immune infiltration, inflammation

Posted Date: February 2nd, 2024

DOI: https://doi.org/10.21203/rs.3.rs-3915790/v1

Additional Declarations: No competing interests reported.

Version of Record: A version of this preprint was published at Apoptosis on April 23rd, 2024. See the published version at https://doi.org/10.1007/s10495-024-01961-6.

Abstract

Objective

Chronic inflammatory and immune responses play key roles in the development and progression of chronic obstructive pulmonary disease (COPD). PANoptosis, as a unique inflammatory cell death modality, is involved in the pathogenesis of many inflammatory diseases. We aim to identify critical PANoptosis-related biomarkers and explore their potential effects on respiratory tract diseases and immune infiltration landscapes in COPD.

Methods

Total microarray data consisting of peripheral blood and lung tissue datasets associated with COPD were obtained from the GEO database. PANoptosis-associated genes in COPD were identified by intersecting differentially expressed genes (DEGs) with genes involved in pyroptosis, apoptosis, and necroptosis after normalizing and removing the batch effect. Furthermore, GO, KEGG, PPI network, WGCNA, LASSO-COX, and ROC curves analysis were conducted to screen and verify hub genes, and the correlation between PYCARD and infiltrated immune cells was analyzed. The effect of PYCARD on respiratory tract diseases and the potential small-molecule agents for the treatment of COPD were identified. PYCARD expression was verified in the lung tissue of CS/LPS-induced COPD mice.

Results

PYCARD was a critical PANoptosis-related gene in all COPD patients. PYCARD was positively related to NOD-like receptor signaling pathway and promoted immune cell infiltration. Moreover, PYCARD was significantly activated in COPD mice mainly by targeting PANoptosis.

Conclusion

PANoptosis-related gene PYCARD is a potential biomarker for COPD diagnosis and treatment.

Introduction

COPD, as a serious chronic lung disease, is characterized by poorly reversible and incomplete airway obstruction[1]. COPD is the third disease in the top 10 causes of death globally and in China [2–3]. COPD was traditionally thought to be influenced by cigarette smoking which causes about half of all COPD cases worldwide[4]. However, the importance of non-cigarette-related risk factors for COPD has strongly increased in recent years, including genetic factors, occupational exposures, air pollution, environmental tobacco smoke, poorly controlled asthma, and infectious diseases[5–6].

Innate and adaptive inflammatory immune is the most common pathogenesis of COPD[7–8]. Multiple immune cells and mediators have been implicated in the inflammatory immune process, which involve innate immune cells (macrophages, neutrophils, mast cells, natural killer cells, dendritic cells, monocytes, eosinophils, and γ/δ-T cells) and adaptive immune cells (T and B cells)[6, 9]. ‘M1-like’ pro-inflammatory macrophages were increased in COPD which involved the strong recruiting of monocytes from the circulation, whereas ‘M2-like’ anti-inflammatory macrophages contributed to defective remodeling in COPD[10–11]. Blood neutrophils were increased in early-stage COPD, and the molecular and functional changes of neutrophils were correlated with the decline of lung functions[12]. Homocysteine elicited a neutrophil apoptosis-to-NETosis shift via the AKT1-S100A8/A9 axis in COPD[13]. It was also the ratio of monocytes, dendritic cells, and natural killer cells increased in COPD patients[14–15]. Moreover, alveolar macrophages (AMs) necroptosis, apoptosis, and pyroptosis contributed to COPD pathogenesis[16–17]. Resting mast cells were significantly decreased[18]. COPD patients have increased neutrophils in sputum and blood, which were associated with more frequent exacerbations[11, 19]. The significantly enhanced expression of γ/δ-T cells and T regulatory cells appeared associated with COPD[20]. These results highlight a novel and crucially important pathogenic mechanism for COPD.

The innate immune system recognizes microbial molecules of pathogens and induces a rapid response by producing inflammatory factors and activating the programmed cell death (PCD) pathway[21]. Recent advances reported a novel inflammatory PCD modality called PANoptosis (pyroptosis, apoptosis, necroptosis)[22]. PANoptosis is a highly interconnected innate immune inflammatory cell death process that is driven through a multiprotein complex (PANoptosome) and involves crosstalk and co-regulation among these cell death pathways[22–23]. PANoptosis plays a crucial role in coronavirus disease 2019 (COVID-19), cancer, metabolic dysfunction-associated fatty liver disease (MAFLD), and acute respiratory distress syndrome (ARDS)[24–27]. Macrophages are an important effector of innate immune cells in PANoptosis[24, 28]. However, the understanding and regulation of PANoptosis in COPD are still revealed.

Our study mainly will demonstrate the association of PANoptosis with COPD. Screening the candidate's biomarkers of PANoptosis and the correlation with immune infiltration in COPD by bioinformatics and validation in COPD mice model analyses, and identifying the effects of the candidate biomarkers in respiratory tract diseases performed by CTD database.

Materials and methods

Data collection

The gene microarray data of COPD samples were mainly collected from Gene Expression Omnibus (GEO, https://www.ncbi.nlm.nih.gov/geo/). The 5 lung tissue datasets (GSE162635, GSE92511, GSE37768, GSE73395, GSE76925) and 5 peripheral blood datasets (GSE112811, GSE103174, GSE54837, GSE133096, GSE55962), containing 365 healthy (control group) and 679 COPD (experimental group) samples were selected. PANoptosis-related genes integrated pyroptosis, apoptosis, and necroptosis

genes that were retrieved from the public GeneCards database (http://www.zhounan.org/ferrdb) The final 96 PANoptosis genes obtained after removing duplicate genes were used for subsequent analysis.

Identification of PANoptosis genes in COPD

The normalized gene expression matrix of the 5 blood/lung tissues datasets after removing batch effects. We first combined the above 10 datasets with limma R package (version 3.42.2) in Silico Merging[DOD:10.1186/1471-2105-13-335]. Then, the obtained merged dataset was analyzed using removal of Batch Effect function of limma R package to remove batch effects, and the data sets before and after normalization were visualized using a boxplot, density graphic, and UMAP chart. Subsequently, linear models were applied to figure out differentially expressed genes (DEGs) between COPD and healthy samples (version 4.3, http://www.bioconductor.org/packages/release/bioc/html/limma.html) Briefly, |log2 fold change (FC)| > 0.99 and $P < 0.05$ were set as the selection criteria for DEGs. the crossover genes between DEGs and 96 PANoptosis genes were identified as PANoptosis genes in COPD. Venn plot, Volcano plot, and Heatmap were conducted and visualized DEGs using the Sangerbox web tool (version 3.0, http://www.theSangerbox.com/home.html)

Functional enrichment analysis of PANoptosis genes in COPD

Functional enrichment analysis was performed on 71 PANoptosis genes in COPD. Gene Ontology (GO) and Kyoto Encyclopedia of Genes and Genomes (KEGG) pathways were used to explore potential biological processes, cellular components, molecular functions, and important signaling pathways. GO and KEGG enrichment analyses were conducted by package cluster Profiler (version 3.14.3). A minimum gene set of 5 and a maximum gene set of 5000 were chosen. $P < 0.05$ and false detection rate (FDR) < 0.1 were considered statistically significant.

Protein-protein interaction (PPI) network construction

Interactions between different PANoptosis genes were analyzed using STRING database (version 11.09, https://cn.string-db.org/) Herein, the "Organism" used was “Homo,” Cytoscape software (version 3.9.1) was used for construction and visualization of PPI networks. The hub genes were identified with Cytoscape plug-in Cytohubba according to the betweenness centrality (BC) of the gene in the PPI network.

Weighted correlation network analysis (WGCNA)

WGCNA is used to mine and find co-expressed gene modules, and it is aimed at exploring the association between the module genes and clinical phenotype. The relative modules in COPD were identified via R package WGCNA (version 1.71, https://cran.r-project.org/web/packages/WGCNA/index.html). At first, MAD (Median Absolute Deviation) was calculated for each gene, and 50% of genes showing the lowest MAD were filtered before further analysis. Then, a weighted adjacency matrix was constructed based on the power function A_mn=|C_mn|^β (C_mn = Pearson's correlation between Gene_m and Gene_n; A_mn = adjacency between

Gene m and Gene n). β was a soft-thresholding parameter. The adjacency was transformed into a topological overlap matrix (TOM), and the corresponding dissimilarity (1-TOM) was calculated after obtaining the power of 16. To classify Genes with similar expression profiles into Gene modules, average linkage hierarchical clustering was conducted according to the TOM-based dissimilarity measure with a minimum size (Gene group) of 30 for the Genes dendrogram. To further analyze the module, we calculated the dissimilarity of module eigengenes, chose a cut line for module dendrogram, and merged some modules. Parame-tersdeepSplit and Similar module merge thresholds were set at 3 and 0.25, respectively. Finally, we obtained 18 co-expression modules.

Least absolute shrinkage and selection operator regression (LASSO) construction

LASSO regression was aimed at constructing a risk model via R package glmnet. K-fold LASSO-Cox regression was implemented after integrating survival time, survival state, and gene expression. Cross-validation (k = 5) was used to obtain and test the model. Correlation coefficients at lambda. min was set as the final model. After candidate genes were selected at lambda. min, R package survival was used to calculate the Risk Score. A prognostic model was conducted using Cox method to evaluate each gene. LASSO-Cox regression was generated using the Sangerbox web tool.

Receiver operating characteristic (ROC) Curve construction

ROC curve was further validated by hub genes and it is aimed at evaluating the diagnostic value of DEGs. The area under the curve (AUC), sensitivities, and 1-specificiies were obtained using R package pROC (version 1.17.0.1). The AUC values are 0.5–0.7/0.7–0.9/ > 0.9 were identified as low/moderate/high accuracy, respectively. Sensitivities and 1-specificities together are used to evaluate the authenticity of the model, they get closer to 1.0, the model is much more authentic.

Immune Infiltration Analysis

Immune infiltration analysis between control and COPD groups was operated by CIBERSORTx web tool (https://cibersortx.stanford.edu/upload.php). CIBERSORTx calculated the composition of 22 types of immune cells in each sample after obtaining the immune cell infiltration matrix, The algorithm employed the LM22 signature for 100 permutations. Filtering out samples with $P < 0.05$ for further analysis. Spearman correlation analysis was carried out to illustrate the correlation within 22 types of immune cells and the association between hub genes and infiltrated immune cells. A bar graph was used to show the distribution of 22 types of immune cell infiltrations in each sample via the Sangerbox web tool. The related heatmap was further applied to visualize the correlation of 22 immune cell infiltrations using a corrplot package. Finally, the correlation between hub genes and infiltrated immune cells was visualized using ggplot2 package. $P < 0.05$ was considered significant.

Connective Map database (CMAP) drug database analyses

The top 150 up-regulated and 150 down-regulated DEGs were uploaded to the CMAP (http://www.broadinstitute.org/cmap/) to investigate the potential small-molecule agents for treatment

of COPD.

PANoptosis-related hub genes all regulatory target gene sets analyses

To predict the regulatory target gene of identified hub genes based on the gene expression profile of patients with COPD, we applied gene set enrichment analysis (GSEA) in the Sangerbox (http://www.theSangerbox.com/home.html), and the c3.all.v7.4.symbols.gmt gene set was downloaded from the Molecular Signatures database, with the threshold set at $P < 0.05$.

Comparative Toxicomics Database (CTD) analyses

The inference scores of PYCARD in a total of 17 types of respiratory tract diseases were analyzed by CTD database (http://ctdbase.org/).

Animal models and experimental procedures

All animal care and experimental protocols were approved by the Animal Experimental Ethical Committee of Kunming Medical University, and all animals received humane care in compliance with the National Institutes of Health guidelines.

The COPD mice model was induced by CS exposure and LPS administration. Briefly, 6-8-week-old male C57BL/6 mice were kept in specific pathogen-free facilities with free access to food and water for 1 week before experiments. After 1 week acclimation period, mice were given 5 μg of LPS by intratracheal instillation under isoflurane anesthesia (Escherichia coli O55:B5, Sigma Aldrich, USA) on week 1. Mice were placed in an oral and nasal exposure system (Beijing Huironghe Technology, China) and exposed to CS (1 cigarettes/1 mouse, once/day, 6 days/week) from 1 to 16 weeks except for the day with LPS administration. The cigarette suction parameters included the following: suction time of 2 s, time interval of 2 s, suction frequency of 10 s, and suction flow of 35 ml. Cigarettes (Hongqi Canal® Filter tip cigarette, smoke of each cigarette containing 11 mg tar, 0.7 mg nicotine, and 13 mg carbon monoxide) were obtained from Henan Tobacco Industry (Zhengzhou, China). The relevant parameters of exposure were as follows: dilution flow of 10 L/min, air extraction flow of 13 L/min, oxygen concentration of 20 ± 0.5%, and air humidity of 60 ± 5%.

Pulmonary Function Examination

Pulmonary function in conscious mice was measured biweekly by whole-body plethysmography (EMKA Technologies, Canada). The respiratory parameters obtained using this technique include Expiratory time (Te), inspiratory time (Ti), relaxation time (RT), expiratory flow at 50% tidal volume (EF50), peak expiratory flow (PEF), peak inspiratory flow (PIF), maximum minute ventilation (MV), expiratory volume (EV).

Invasive lung function was assessed with a FlexiVent system (SCIREQ, Montreal, Canada). A plastic cannula was inserted into mouse tracheas and connected to the FlexiVent system. Vecuronium bromide (6 mg/kg) was injected intraperitoneally to maintain muscle relaxation. Then, mechanical ventilation was

initiated to measure Newtonian resistance (Rn), respiratory resistance (Rrs), compliance respiratory system (Crs), static compliance (Cst), forced expiratory volume in 0.1 s (FEV0.1), forced expiratory volume in 0.2 s (FEV0.2), forced expiratory volume in 0.05 s (FEV0.05), forced vital capacity (FVC), forced expiratory volume in 0.1 s/forced vital capacity (FEV0.1/FVC), forced expiratory volume in 0.2 s/forced vital capacity (FEV0.2/FVC), and forced expiratory volume in 0.05 s/forced vital capacity (FEV0.05/FVC). The data obtained were analyzed using the FlexiVent software (SCIREQ, Montreal, Canada).

Hematoxylin-eosin (H&E) and Masson staining

Lung tissues of the mice were fixed using 4% paraformaldehyde and embedded in paraffin followed by sectioning into 5 μm sections, and the sections were placed on glass slides, deparaffinized, and subjected to hematoxylin and eosin (H&E). For analysis of collagen deposition in lung tissues, paraffin sections were stained with Sirius red and Massons trichrome, and counterstained with Mayers Hematoxylin. The pathological characteristics of the tissues were evaluated via light microscopy.

Western blot analysis

Lung tissues from each mouse were homogenized in lysis buffer (RIPA: Cocktail: PMSF: Phosstop = 0.657: 0.143: 0.1: 0.1) to extract total protein. Lung proteins (30 μg) were loaded onto 10% SDS-PAGE and transferred to PVDF membranes (Millipore Corporation, Billerica, MA). The membranes were blocked for 1 h with TBST supplemented with 5% non-fat dry milk at room temperature, and then incubated overnight at 4°C with anti-PYCARD (Cell Signalling Technology, MA, USA), or anti-β-actin (Cat. #93473, Cell Signalling Technology, MA, USA). The membranes were washed thrice with TBST and then incubated for 2 h at room temperature with a horseradish peroxidase-conjugated secondary antibody. The membranes were again washed thrice with TBST and then developed using an enhanced chemiluminescent detection kit (Cat.WBKLS0500, Millipore Corporation, Billerica, MA). The density of the protein bands in the membrane was quantified by Scion Image 4.0.2 (Informer Technologies, USA).

Statistical analysis

All Data were displayed as mean ± SEM. The Student's t-test was used for comparison between two groups and Student-Newman-Keuls was selected for analyses. One-way ANOVA was employed for comparison between multiple groups, lung function and body weight between control group and COPD mice in different time points were compared using the Two-way analysis of variance (ANOVA), and then Turkey test was selected for analyses, $P < 0.05$ was considered significant. All the statistical analyses were conducted using GraphPad Prism 8.0 software.

Results

Identifying PANoptosis-associated DEGs in COPD

We first screened 5 blood and 5 lung datasets for DEGs from GEO database with the R package limma (Fig. 1). Next, we acquired a merged expression profile after removing the batch effect of COPD from 5

blood/5 lung datasets (Fig S1). We then obtained 96 PANoptosis-related genes from the overlapping genes in apoptosis, necroptosis, and pyroptosis. These genes were downloaded from the public GeneCards database (Fig. 2A). We narrowed the list and identified 71 PANoptosis-related genes of COPD presented in all 3 groups (Fig. 2B). The expression levels of these 71 overlapping PANoptosis-related genes in COPD and normal samples were presented as a Volcano plot (Fig. 2C).

Functional enrichment analysis of 71 PANoptosis-related genes in COPD

To explore the biological functions and signal transduction pathways of the 71 candidate PANoptosis genes, we performed GO and KEGG enrichment analysis (Fig. 3A). Subsequently, GO enrichment analysis illustrated these PANoptosis genes were primarily associated with different significant BP (Fig. 3B), CC (Fig. 3C), and MF (Fig. 3D), respectively. These top 20 GO terms in BP, CC, and MF were shown in Fig. 3E, mainly including regulation of cell death, cellular response to chemical stimulus, response to chemical, positive regulation of protein metabolic process, regulation of cytokine production, immune system process, and oxygen-containing compound. The pathway enrichment analysis revealed that PANoptosis genes were mainly enriched in COPD and associated with NOD-like receptor signaling pathway, necroptosis, apoptosis-multiple species, TNF signaling pathway, IL-17 signaling pathway, Toll-like receptor signaling pathway, cytosolic DNA-sensing pathway, NF-κB signaling pathway, p53 signaling pathway, C-type lectin receptor signaling pathway, MAPK signaling pathway, T cell receptor signaling pathway, Th17 cell differentiation, Ubiquitin mediated proteolysis, B cell receptor signaling pathway, Th1 and Th2 cell differentiation, and ferroptosis (Fig. 3F).

Constructing the network of optimized PANoptosis-related DEGs in COPD

According to the expression profile from the COPD dataset, we observed that there were 25 significant PANoptosis-related DEGs in COPD, including BAX, HMGB1, MAPK14, CASP1, NLRP3, CASP6, GJA1, IKBKE, RIPK1, CDK1, SQSTM1, RIPK3, ZBP1, TRAF3, MLKL, PKM, TRIM24, BECN1, BNIP3, DDX3X

PYCARD, MYD88, TP63, AIM2, UBE2D3. Among the 25 optimized PANoptosis DEGs, BAX, MAPK14, CASP1, NLRP3, IKBKE, RIPK1, SQSTM1, RIPK3, ZBP1, TRAF3, MLKL, PKM, BECN1, PYCARD, MYD88, TP63, AIM2, and UBE2D3 were highly expressed in COPD versus normal samples. By contrast, the other 7 DEGs had lower expression in tumors than in normal tissue (Fig. 4A-B). The PPI network constructed and screened 15 optimized candidates (Fig. 4C).

Screening the relative module genes in COPD

WGCNA was applied to screen the relative modules in the external validation set (GSE76925), and a threshold power of β = 3 was systematically selected to construct the scale-free network, while R^2 cut at 0.86 (Fig. 5A-B). WGCNA identified 13 modules, where tan and blue modules (module trait correlation =

0.24 and 0.18) had a strong positive correlation with COPD, while turquoise modules (-0.18) were negatively connected to COPD (Fig. 5C-D). As shown in the scatter plot (Fig. 5E-G), all significant members in the 3 key modules with COPD genes were cor = 0.32, *P* = 7.0e-30, cor = 0.54, *P* = 5.7e-8, cor =-0.71, *P* = 0.0e-0, respectively.

Prognosis analysis of optimized PANoptosis-related genes in COPD

In addition, we verified candidate diagnostic biomarkers utilizing LASSO logistic regression algorithm to identify COPD-related feature variables of the 15 optimized DEGs (Fig. 6A-B). The diagnostic validity of the PANoptosis genes was validated by AUC of risk score (Fig. 6C). To explore the relationship of the candidate PANoptosis DEGs with patient prognosis, we used multivariate Cox regression analysis to identify 6 prognostic PANoptosis DEGs (MAPK14, BAX, CASP1, TP63, PYCARD, DDX3X) associated with COPD (Fig. 6D).

Validating hub PANoptosis-related genes in COPD

Furthermore, ROC curve was visualized and illustrated the diagnostic validity of 6 diagnostic markers. ROC analysis of the genes was performed based on the merged COPD dataset (Fig. 7A). The 6 diagnostic markers had an AUC (> 0.50), and their expression was visualized by a volcano diagram in the merged expression profile (Fig. 7B). Moreover, we analyzed and estimated the level of the 6 diagnostic markers in COPD patients and normal samples. As shown in Fig. 7C, MAPK14, BAX, CASP1, and PYCARD, had outstanding *P*-values (< 0.05).

Determining if the target PYCARD in COPD

The intersection of 4 optimized PANoptosis-related genes (MAPK14, BAX, CASP1, and PYCARD) and 3 related modules (tan, blue, turquoise) of significant genes are presented in Venn diagram. The 4 overlapped PANoptosis-related genes were identified for further analysis, including MAPK14, BAX, CASP1, and PYCARD (Fig. 8A). Moreover, the degrees of correlations of the 4 candidates' PANoptosis genes and COPD with normal patients were shown by a scatter plot. However, only PYCARD had a significant *P*-value (2.3e-25) (Fig. 8B-E), of which the expression level was dramatically up-regulated in COPD compared with that of the normal group (Fig. 8F).

Difference analysis and enrichment analysis of PYCARD grouping

The merged expression profile of 5 blood/lung COPD datasets, after removal of batch effect, was divided into a low-expression group and a high-expression group according to the median value of PYCARD, with *P* < 0.05 and |log2FC| >0.99. 2325 significant low-expressed genes and 3460 high-expressed genes were

collected (Fig. 9A). The heatmap only showed the top 20 low- and high-DEGs in |logFC| order, respectively (Fig. 9B).

Subsequently, we studied the functional effects of different PYCARD expressions based on GO and KEGG enrichment analysis. The top 20 types of GO analysis primarily contained protein modification process, cellular response to chemical stimulus, leukocyte activation, positive regulation of metabolic process, regulation of response to stimulus, immune system process, phosphorylation, cell surface receptor signaling pathway, cell death, neutrophil activation, granulocyte activation, T cell activation, ubiquitin-like protein ligase binding. These enrichments clearly show that the expression of PYCARD was closely related to cell death, immune system process, and protein modification (Fig. 9C). KEGG pathway, which displayed Metabolic pathway, TNF signaling pathway, Lysosome, Chemokine signaling pathway, p53 signaling pathway, C-type lectin receptor signaling pathway, MAPK signaling pathway, T cell receptor signaling pathway, FoxO signaling pathway, NF-κB signaling pathway, Th17 cell differentiation, Phospholipase D signaling pathway, Ferroptosis, NOD-like receptor signaling pathway, was mainly related to PYCARD grouping in COPD. These pathways were also mostly related to inflammation, oxidative stress, ferroptosis, and T cell receptor signaling pathway (Fig. 9D).

Analyzing the correlation between PYCARD and immune-infiltrated cells in COPD

CIBERSORT algorithm was used to confirm the correlation between PYCARD expression and immune cells, and we first analyzed the proportion of 22 types of immune cells in COPD samples (Fig S2A). The correlation of 22 types of infiltrated immune cells was constructed with a correlation heatmap (Fig S2B). 9 types of significantly different infiltration immune cells in patients with COPD and controls were visualized (Fig. 10A). B cells naive, T cells CD8, T cells CD4 memory activated, and Mast cells activated were negatively connected to COPD, but T cells CD4 naive, Dendritic cells resting, Macrophages M0, Mast cells activated, and Eosinophils had a positive correlation with COPD. The correlation analysis between PYCARD and infiltrated immune cells illustrated that a total of 17 kinds of immune cells had significant correlations with PYCARD (Fig. 10B). We also analyzed the relationship between PYCARD and 3 types of primary immune infiltration cells that were consistent with the COPD, including T cells CD4 memory activated (r = -0.16, P = 7.4e-5), Dendritic cells resting (r = 0.23, P = 1.2e-8), and Macrophages M0 (r = 0.27, P = 2.3e-11) (Fig. 10C).

The effect of PYCARD on respiratory tract diseases

The correlation between PYCARD and a total of 17 types of respiratory tract diseases under chemical or environmental exposure was displayed by a comparative toxicogenomics database (CTD). The respiratory tract diseases contain lung diseases, respiratory tract diseases, lung diseases (interstitial and obstructive), respiratory tract infections, bronchial diseases, respiration disorders, pneumonia, respiratory distress syndrome, acute lung injury, respiratory insufficiency, idiopathic pulmonary fibrosis, pleural disease, bronchial hyperreactivity, pulmonary edema, pulmonary disease, and COPD. The

inference score of PYCARD in lung diseases was the highest, and also high in COPD (Fig. 11). The results implied that PYCARD might be a potential treatment target for multiple lung diseases.

The analysis of the potential drugs for COPD

Based on the target PYCARD in COPD, we further investigated the potential drugs and targeting pathways using the CMAP database. The top 50 key mechanisms of treating COPD and relevant drugs were analyzed by normal connectivity scores. The mechanism of Tublin inhibitor, Topoisomerase inhibitor, DNA inhibitor Aurora kinase inhibitor, and Histamine receptor inhibitor was dramatically enriched by targeting related genes (Fig. 12). These findings could provide new ideas for the treatment of COPD.

Predicting potential target genes for PYCARD in COPD

PYCRD might play a critical role in inflammation and immune process in COPD. The potentially key target genes of PYCARD were therefore evaluated based on the merged expression profile of COPD (Fig. 13A). The top 5 positive and negative target genes of PYCARD were found by GSEA analysis. These findings implied PYCARD might regulate COPD by increasing the expression levels of ADNP, CDH4, MCM2, PU1, and DPPA3 (Fig. 13B), whereas decreasing those of CEBP_C, CDPCR3, OCT1, EVI1, and HFH3 (Fig. 13C).

PYCARD was up-regulated in CS/LPS-induced COPD mice

We observed that the key gene of PANoptosis-PYCARD dramatically increased in COPD patients (Fig. 7C). To further increase our confidence in the findings, the expression of PYCARD was further validated in the CS/LPS-induced COPD mice model. The lung function in conscious mice was detected every two weeks, Te, Ti, and RT increased while EF50, PEF, PTF, MV, and EV decreased in model mice from 6 to 16 weeks, compared with the control group (Fig. 14A). Meanwhile, invasive lung function showed that CS exposure decreased the lung function ventilation parameter Crs, Cst, fFEV0.1, FEV0.2, FEV0.05, FVC, FEV0.1/FVC, FEV0.2/FVC, and FEV0.05/FVC and increased the resistance parameters Rn and Rrs in COPD mice (Fig. 14B). In addition, lung sections from COPD model mice slightly increased the number of inflammatory cells, alveolar wall thickening, and mucus-producing (Fig. 14C). As shown in Fig. 14A, The lung tissue of control group mice exhibited only little collagen fiber deposition around vessels and bronchioles. However, extensive collagen was readily observed in lung tissue of CS group mice compared with the control group, which confirmed CS-induced fibrosis in lung tissue. Furthermore, compared with the control group, the body weight was significantly decreased in model mice (Fig. 14D). The results indicated that CS exposure decreased lung function and aggravated the pathological changes in model mice.

Lastly, we found that the expression of PANoptosis-related proteins including Caspase3, NLRP3, and p-MLKL was significantly increased in lung tissue of COPD mice (Fig. 15A). Meanwhile, the protein expression of PYCARD was markedly higher in lung tissues from CS/LPS-treated mice than the control

mice (Fig. 15B). These results suggest that PYCARD acts at least partly via PANoptosis, and may contribute to the inflammatory responses of COPD.

Discussion

COPD is one of the leading causes of death nationally and even worldwide[29–30]. A prolonged time constant for lung emptying leads to airflow limitation in COPD, which is caused by the increased compliance of the lung as a result of emphysematous destruction and the elevated resistance of small conducting airways[31–32]. These lesions are associated with the host's lifetime response to inhalation of toxic gases and/or particles, as well as result in a chronic innate and adaptive inflammatory immune response[33–35]. PANoptosis is a newly programmed cell death modality that enables crosstalk and coordination among pyroptosis, apoptosis, and necroptosis pathways, which is strongly associated with immune inflammation[36]. However, the roles of PANoptosis-related genes (PRGs) in the development and immune landscape of COPD remain widely unclear. Thus, using previously published data, we explored the effect of PANoptosis-related genes in immune infiltration and its underlying mechanisms in COPD. Above all, the overall regulation of PANoptosis in COPD was elucidated.

In the present study, we identified 71 PANoptosis-related genes after integrating the lung-related DEGs with blood-related DEGs in COPD datasets, based on the previously obtained 96 PANoptosis-related genes. Subsequently, function enrichment analysis showed that most biological processes were enriched in programmed cell death, cytokine production, immune system process, response to chemical stimulus, and the most enrichment pathways were involved in TNF signaling pathway, Toll-like receptor signaling pathway, B cell receptor, and T cell receptor signaling pathway. These processes and pathways were widely involved in the development of COPD[37–39]. These results also indicated that PANoptosis-related genes were the key regulator of inflammatory and immune responses. Next, we evaluated the diagnostic value of PANoptosis-related genes in COPD through LASSO-COX regression and ROC curves analysis, which displayed a dramatic increase in the expression of BAX, MAPK14, CASP1, and PYCARD in COPD patients. It was also validated that these PANoptosis-related genes were the key module members by WGCNA analysis. Furthermore, the expression of PYCARD was significantly increased in COPD patients. These findings illustrated that PYCARD could be a novel and potential biomarker for COPD. The inflammasome adaptor protein PYCARD (known as ASC) is a potential pyroptosis biomarker engaged in inflammation and related to immune response[40], which provides new insights into the pathogenesis of inflammatory diseases[41–42]. In addition, regarding function enrichment analysis, we demonstrated that PYCARD was mainly related to protein modification process, chemical stimulus, regulation of response to stimulus, and immune system process. Remarkably, PYCARD was engaged in metabolic pathways, TNF signaling pathway, and C-type lectin receptor signaling pathway. These results also illustrated that the PANoptosis-promoting role of PYCARD in COPD might regulate the above biological processes and signaling pathways.

Immune cells in the innate immune response play a key role in COPD and inflammation[43]. PANoptosis is also significantly associated with the innate immune[21]. To better grasp the infiltrated immune cells

of COPD and the correlation with PYCARD, we constructed the immune infiltration analysis and found that B cells naive, T cells CD8, T cells CD4 naive, T cells CD4 memory activated, macrophages M0, dendritic cells resting, mast cells activated, and neutrophils were remarkably associated with COPD. Meanwhile, the immune-related analysis further indicated that PYCARD affected many immune cells. In particular, we noticed that macrophages M0 and dendritic cells resting with high PYCARD expression, T cells CD4 memory activated had a negative correlation with the PYCARD level. These findings showed that most innate immune regulators had a positive association with the PYCARD. Meanwhile, PYCARD played a critically positive role in COPD, which might be exerted by regulating the above immune cells.

In addition, we uncovered the most enrichment target genes of PYCARD based on GSEA analysis, including HNF4, CAVIN1, PU.1, DPPA3, and SIRT3. Hepatocyte nuclear factors 4 (HNF4) were involved in metabolism, cell junctions, differentiation, and proliferation and thus regulate liver and intestinal inflammatory networks[44–45]. Caveolae-associated protein 1 (CAVIN1) controls lipid distribution and inflammatory signaling by modulating macrophage number, phenotype and oxidative stress[46–48]. Transcription factorSpi-1/PU.1 plays an important role in the differentiation of immune cells. PU.1 expression increased during granulocyte and macrophage differentiation, while decreased during T lymphocyte and B lymphocyte differentiation[49]. PU.1 promotes the development of rheumatoid arthritis by inducing the hyperactivation and inflammatory status of macrophages[50]. DPPA3 (known as PGC7) modulates promoter demethylation of genes related to development[51]. SIRT3 could function as a regulator against cardiovascular diseases, aging-related diseases, and liver diseases[52–54]. These potential target genes indicated a positive relationship with the PYCARD expression. However, further investigation is still required to verify the specific role of PYCARD in COPD and reveal the potential mechanisms.

Conclusions

In summary, we applied a comprehensive bioinformatics analysis and a multi-omics approach to characterize the functional role of PANoptosis genes and their association with the immune landscape in COPD patient samples. We demonstrated that the occurrence and progression of COPD are closely related to PANoptosis. We also identified the PANoptosis-related gene PYCARD associated with COPD inflammation, immune responses, C-type lectin receptor signaling pathway, and metabolic pathway. Therefore, we suggest that PYCARD could be utilized as a potential diagnostic biomarker and therapeutic target for COPD.

Declarations

Ethics approval statement

This study was approved by the Medical Ethical Committee of Kunming Medical University. All the experimental methods were carried out according to the approved guidelines. (Approval No. kmmn20230944). All experimental procedures involving mice were carried out in strict accordance

with the recommendations in the Guide for the National Institutes of Health guide for the care and use of Laboratory animals (NIH Publications No. 8023, revised 1978)

Acknowledgments

Rui Shi designed and performed experiments, analyzed the data, and wrote the paper.
Renwen Liang and Fang Wang performed partial experiments. Lueli Wang helped to analyze partial data and revise the manuscript. Wuyi Zidai and Jie Zhang helped to acquire partial data. Luo Min, Xiaohua Du, and Shibo Sun helped to revise the manuscript. Chuang Xiao and Chaozhong Li reviewed the manuscript. Xuewu Liang and Alex F Chen helped to revise the manuscript and gave final approval for the version to be published. Weimin Yang supervised the study, revised it, and reviewed the manuscript. All authors read and approved the final manuscript. We also thank the GEO and HPA research network for providing the data analyzed in this article.

Acknowledgments

This work was funded by the National Natural Science Foundation of China (No. 81870037, 82160013, 82160007); Science and Technology Program of Yunnan Province (No.202105AF150015, 202102AA310030, 202302AA310026); Kunming Development and Reform Commission (202202); State Key Laboratory of Drug Research (SKLDR-2023-KF-08); Yunnan Key Laboratory of Pharmacology for Natural Products (YKLPNP-K2403). In addition, this study was supported in part by the Ministry of Science and Technology of China (2021YFA0804803), the Major Project of Natural Science Foundation of Hunan Province (Open Competition) (2021JC0002), and the National Science Foundation of China (81930012, 82241027).

No conflict of interest

No conflict of interest exists in the submission of this manuscript, and the manuscript is approved by all authors for publication. I would like to declare on behalf of my co-authors that the work depicted was original research that has not been published previously and is not under consideration for publication elsewhere, in whole or in part. All the authors listed have approved the manuscript that is enclosed.

Declaration of Competing Interest

The authors declare no conflicts of interest.

Data availability statement

The data in the current study are available from the first author upon reasonable request.

References

1. Pj B, Pg B, Ek S et al (2015) Chronic obstructive pulmonary disease. Nat Rev Dis Primers 1:15076
2. Leading causes of death and disability 2000–2019: A visual summary. Available from: https://www.who.int/data/stories/leading-causes-of-death-and-disability-2000-2019-a-visual-summary
3. Top 10 causes of death in China for both sexes aged all ages (2019) Available from: https://www.who.int/data/gho/data/themes/mortality-and-global-health-estimates/ghe-leading-causes-of-death
4. Ia Y, Cr J, Ss S (2022) Chronic obstructive pulmonary disease in never-smokers: risk factors, pathogenesis, and implications for prevention and treatment. Lancet Respir Med 10(5):497–511
5. Ek S (2020) Genetics of COPD. Annu Rev Physiol 82:413–431
6. Z Y, B C (2022) Multi-omics analyses of airway host-microbe interactions in chronic obstructive pulmonary disease identify potential therapeutic interventions. Nat Microbiol 7(9):1361–1375
7. Jl S, Jh R, C G et al (2021) The aging lung: Physiology, disease, and immunity. Cell 184(8):1990–2019
8. C B, N G. Airway inflammation in COPD: progress to precision medicine. Eur Respir J. (2019) ;54(2)
9. Kf B, Sd S, Sf R et al (2019) Functional effects of the microbiota in chronic respiratory disease. Lancet Respir Med 7(10):907–920
10. Sv C, Df R (2003) Impaired inhibition by dexamethasone of cytokine release by alveolar macrophages from patients with chronic obstructive pulmonary disease. Am J Respir Crit Care Med 167(1):24–31
11. Pj B (2019) Inflammatory endotypes in COPD. Allergy 74(7):1249–1256
12. Ts K (2023) Systemic alterations in neutrophils and their precursors in early-stage chronic obstructive pulmonary disease. Cell Rep 42(6):112525
13. Y WL (2023) Airway dysbiosis accelerates lung function decline in chronic obstructive pulmonary disease. Cell Host Microbe 31(6):1054–1070
14. Y P (2022) Combining single-cell RNA sequencing of peripheral blood mononuclear cells and exosomal transcriptome to reveal the cellular and genetic profiles in COPD. Respir Res 23(1):260
15. Tm GGG (2022) The arginine methyltransferase PRMT7 promotes extravasation of monocytes resulting in tissue injury in COPD. Nat Commun 13(1):1303
16. Van Eeckhoutte ZL (2021) Necroptosis signaling promotes inflammation, airway remodeling, and emphysema in chronic obstructive pulmonary disease. Am J Respir Crit Care Med 204(6):667–681
17. D ET SF (2023) Immunity against Moraxella catarrhalis requires guanylate-binding proteins and caspase-11-NLRP3 inflammasomes. Embo J 42(6):e112558
18. D W, B C, S B, et al. Screening and identification of tissue-infiltrating immune cells and genes for patients with emphysema phenotype of COPD. Front Immunol. (2022) ;13:967357
19. K M, R K, K G. Eosinophils in COPD-current concepts and clinical implications. J Allergy Clin Immunol Pract. (2020) ;8(8):2565–2574

20. Jm JPJS (2005) Blunted gamma delta T-lymphocyte response in chronic obstructive pulmonary disease. Eur Respir J 25(3):441–446
21. S L, R K, Y W, et al. AIM2 forms a complex with pyrin and ZBP1 to drive PANoptosis and host defence. Nature. (2021) ;597(7876):415–419
22. N BS (2023) NLRP12-PANoptosome activates PANoptosis and pathology in response to heme and PAMPs. Cell 186(13):2783–2801
23. Re SC, Td T (2022) Programming inflammatory cell death for therapy. Pharmacol Ther 232:108010
24. S RK (2022) ZBP1-dependent inflammatory cell death, PANoptosis, and cytokine storm disrupt IFN therapeutic efficacy during coronavirus infection. Sci Immunol 7(74):eabo6294
25. B RK, Br S (2021) ADAR1 restricts ZBP1-mediated immune response and PANoptosis to promote tumorigenesis. Cell Rep 37(3):109858
26. Y M, E C, S R, et al. STING agonist diABZI induces PANoptosis and DNA mediated acute respiratory distress syndrome (ARDS). Cell Death Dis. (2022) ;13(3):269
27. Xt JT, Z L (2023) Ferroptosis inhibitor liproxstatin-1 alleviates metabolic dysfunction-associated fatty liver disease in mice: potential involvement of PANoptosis. Acta Pharmacol Sin 44(5):1014–1028
28. M Z, R K, P V, et al. Caspase-6 is a key regulator of innate immunity, inflammasome activation, and host defense. Cell. (2020) ;181(3):674–687
29. D A, P S, Y Z, et al. Global, regional, and national prevalence of, and risk factors for, chronic obstructive pulmonary disease (COPD) in 2019: a systematic review and modelling analysis. Lancet Respir Med. (2022) ;10(5):447–458
30. GBD Chronic Respiratory Disease Collaborators (2020) Prevalence and attributable health burden of chronic respiratory diseases, 1990–2017: a systematic analysis for the Global Burden of Disease Study 2017. Lancet Respir Med 8(6):585–596
31. Fj M, Br AA (2022) Treatment trials in young patients with chronic obstructive pulmonary disease and pre-chronic obstructive pulmonary disease patients: Time to move forward. Am J Respir Crit Care Med 205(3):275–287
32. Em D, Bm E (2021) Mucus plugs and emphysema in the pathophysiology of airflow obstruction and hypoxemia in smokers. Am J Respir Crit Care Med 203(8):957–968
33. S W, L O, S D, et al. Multi-omics links IL-6 trans-signalling with neutrophil extracellular trap formation and Haemophilus infection in COPD. Eur Respir J. (2021) ;58(4)
34. Js Z, Zy L, Xc X et al (2020) Cigarette smoke-initiated autoimmunity facilitates sensitisation to elastin-induced COPD-like pathologies in mice. Eur Respir J. ;56(3)
35. G C, P C, A B, et al. COPD Immunopathol Semin Immunopathol. (2016) ;38(4):497–515
36. D Y, Y X (2022) Anti-PANoptosis is involved in neuroprotective effects of melatonin in acute ocular hypertension model. J Pineal Res 73(4):e12828

37. K JA (2019) PRKN-regulated mitophagy and cellular senescence during COPD pathogenesis. Autophagy 15(3):510–526
38. M SM, Li JK (2022) A, Plasma proteins elevated in severe asthma despite oral steroid use and unrelated to Type-2 inflammation. Eur Respir J. ;59(2)
39. Pathview. Available from: https://pathview.uncc.edu/guest
40. Jq S, X T, Wh X et al (2022) The inflammasomes adaptor protein PYCARD is a potential pyroptosis biomarker related to immune response and prognosis in clear cell renal cell carcinoma. Cancers. ;14(20)
41. C V, Bs SK (2017) Microglia-derived ASC specks cross-seed amyloid-β in Alzheimer's disease. Nature 552(7685):355–361
42. Kj PDHK (2010) NLRP3 inflammasomes are required for atherogenesis and activated by cholesterol crystals. Nature 464(7293):1357–1361
43. U R (2020) Distribution of ACE2, CD147, CD26, and other SARS-CoV-2 associated molecules in tissues and immune cells in health and in asthma, COPD, obesity, hypertension, and COVID-19 risk factors. Allergy 75(11):2829–2845
44. Jp B (2014) Hepatocyte nuclear factor 4-alpha involvement in liver and intestinal inflammatory networks. World J Gastroenterol 20(1):22–30
45. V D, B S, P L, et al. Control of cell identity by the nuclear receptor HNF4 in organ pathophysiology. Cells. (2020) ;9(10)
46. Jy L, Wn B, Ak M et al (2020) Stromal CAVIN1 controls prostate cancer microenvironment and metastasis by modulating lipid distribution and inflammatory signaling. Mol Cancer Res 18(9):1414–1426
47. W H (2022) Cavin-1 promotes M2 macrophages/microglia polarization via SOCS3. Inflamm Res 71(4):397–407
48. Yw YW, Da L (2023) Caveolae sense oxidative stress through membrane lipid peroxidation and cytosolic release of CAVIN1 to regulate NRF2. Dev Cell 58(5):376–397
49. G L, W H, W H. Transcription factor PU.1 and immune cell differentiation (Review). Int J Mol Med. (2020) ;46(6):1943–1950
50. W JT (2023) PU.1 promotes development of rheumatoid arthritis via repressing FLT3 in macrophages and fibroblast-like synoviocytes. Ann Rheum Dis 82(2):198–211
51. Q Y (2021) PGC7 promotes tumor oncogenic dedifferentiation through remodeling DNA methylation pattern for key developmental transcription factors. Cell Death Differ 28(6):1955–1970
52. T Z (2020) SIRT3 promotes lipophagy and chaperon-mediated autophagy to protect hepatocytes against lipotoxicity. Cell Death Differ 27(1):329–344
53. Y G, X J, Y C, et al. Sirt3-mediated mitophagy regulates AGEs-induced BMSCs senescence and senile osteoporosis. Redox Biol. (2021) ;41:101915

54. M PG (2022) Salt-Induced Hepatic Inflammatory Memory Contributes to Cardiovascular Damage Through Epigenetic Modulation of SIRT3. Circulation 145(5):375–391

Figures

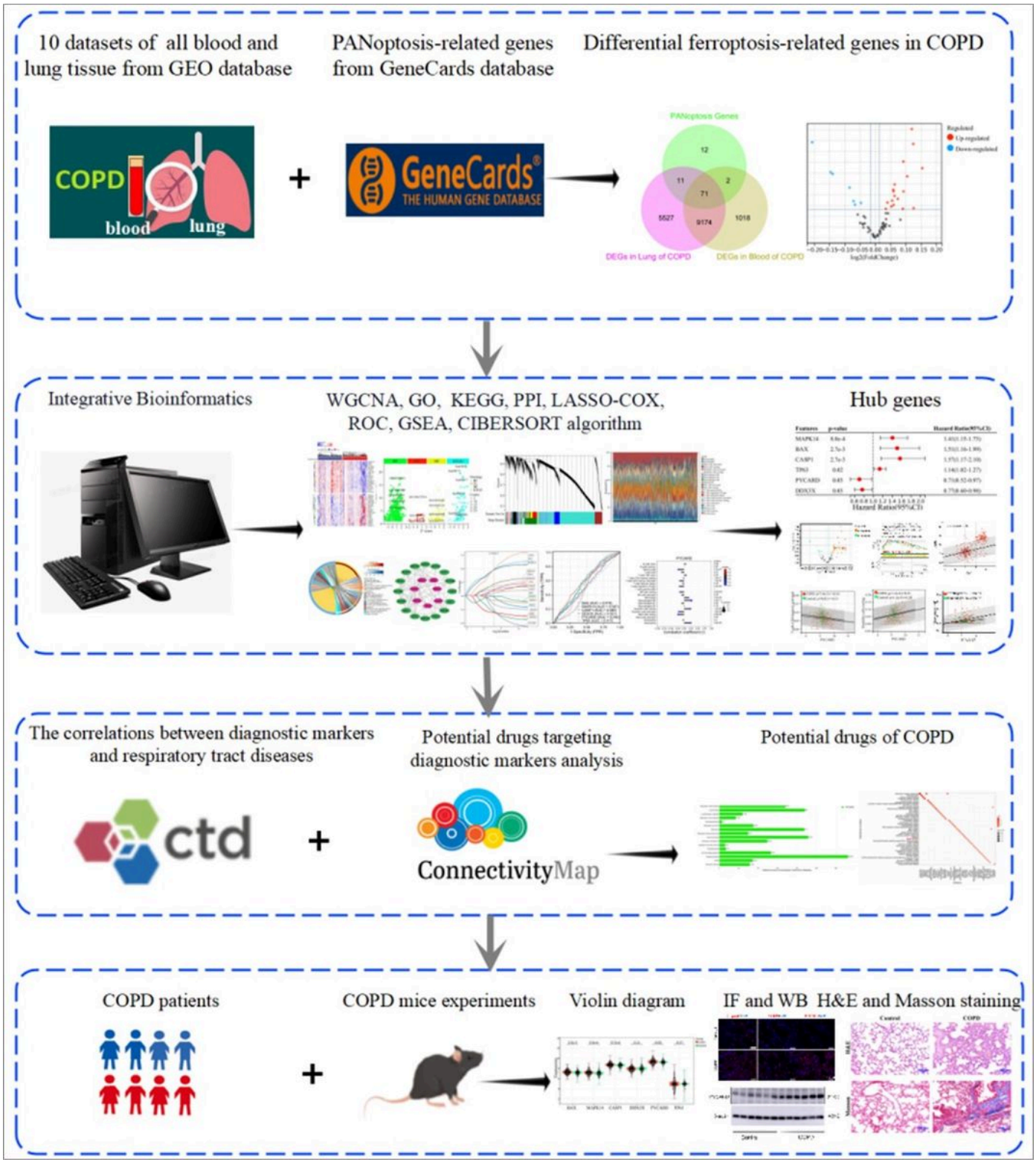

Figure 1

Flowchart of the research.

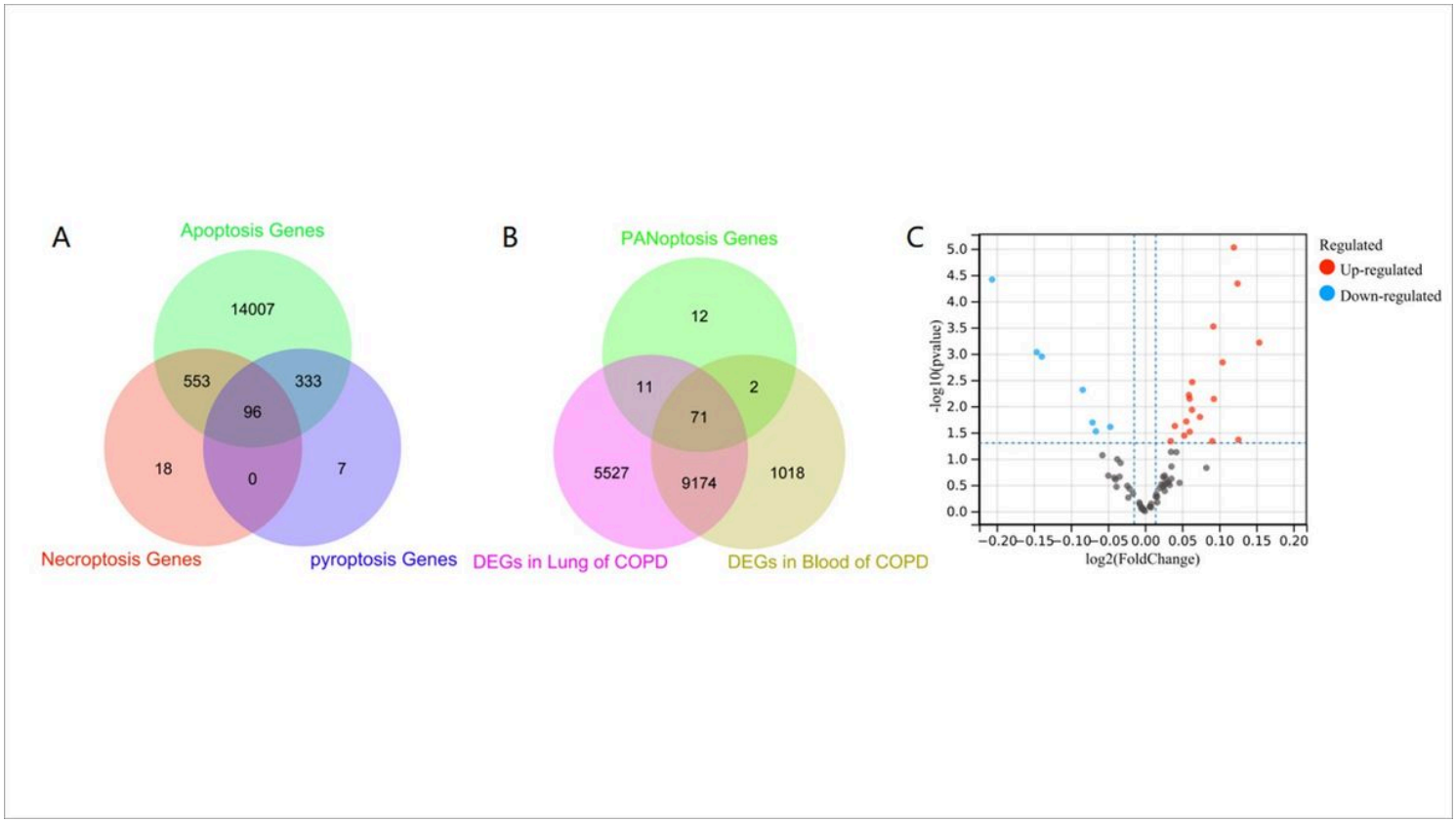

Figure 2

Identification of PANoptosis genes in COPD. A. Venn diagram showing the intersection of Apoptosis genes, necroptosis genes, and pyroptosis genes. The overlapping genes were identified as PANoptosis genes. **B.** Venn diagram showing the PANoptosis genes in COPD by intersecting of 96 PANoptosis genes, DEGs in 5 lung and 5 blood datasets of COPD. **C.** Volcano plots of 71 PANoptosis genes in the merged COPD dataset after removing batch effect with $P < 0.05$ and |log2 fold change (FC)| > 0.99. Up-regulated genes are labeled in red, and down-regulated genes are marked in blue.

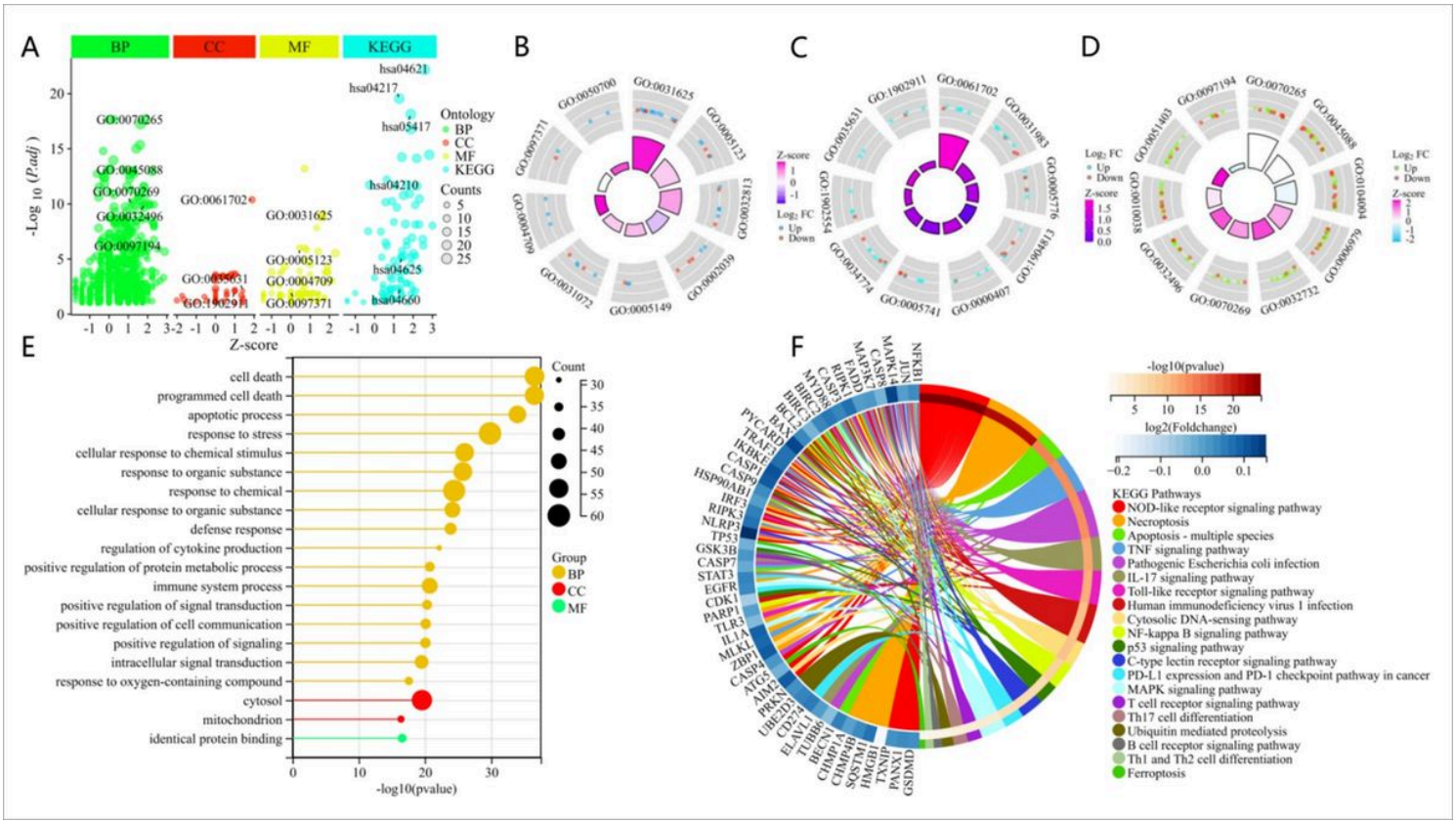

Figure 3

Functions and pathways analysis in 71 PANoptosis genes of COPD. A. GO (containing subsections of biological processes, cellular component, and molecular functions) and KEGG significant terms explained by bubble plot. Bubble plot of each term combined with logFC. The absolute value of the Z-score indicates the probability of regulation, the Z-score greater than zero represents positive regulation, and the Z-score less than zero represents negative regulation. and the size of the dot indicates the number of gene counts. **B-D.** Donut plot represents the top 10 BP, CC, and MF in GO enrichment, respectively. Donut plot of significant terms combined with logFC. Each column of the inner and outer circle corresponds to one term. color indicates logFC value in the outer circle. In the outer circle, the height of column represents adjusted P value, and the filled color represents Z-score of each term. **E.** Top 20 BP, CC, and MF in GO enrichment using a lollipop diagram. **F.** Top 20 KEGG enrichment among these genes using loop diagram.

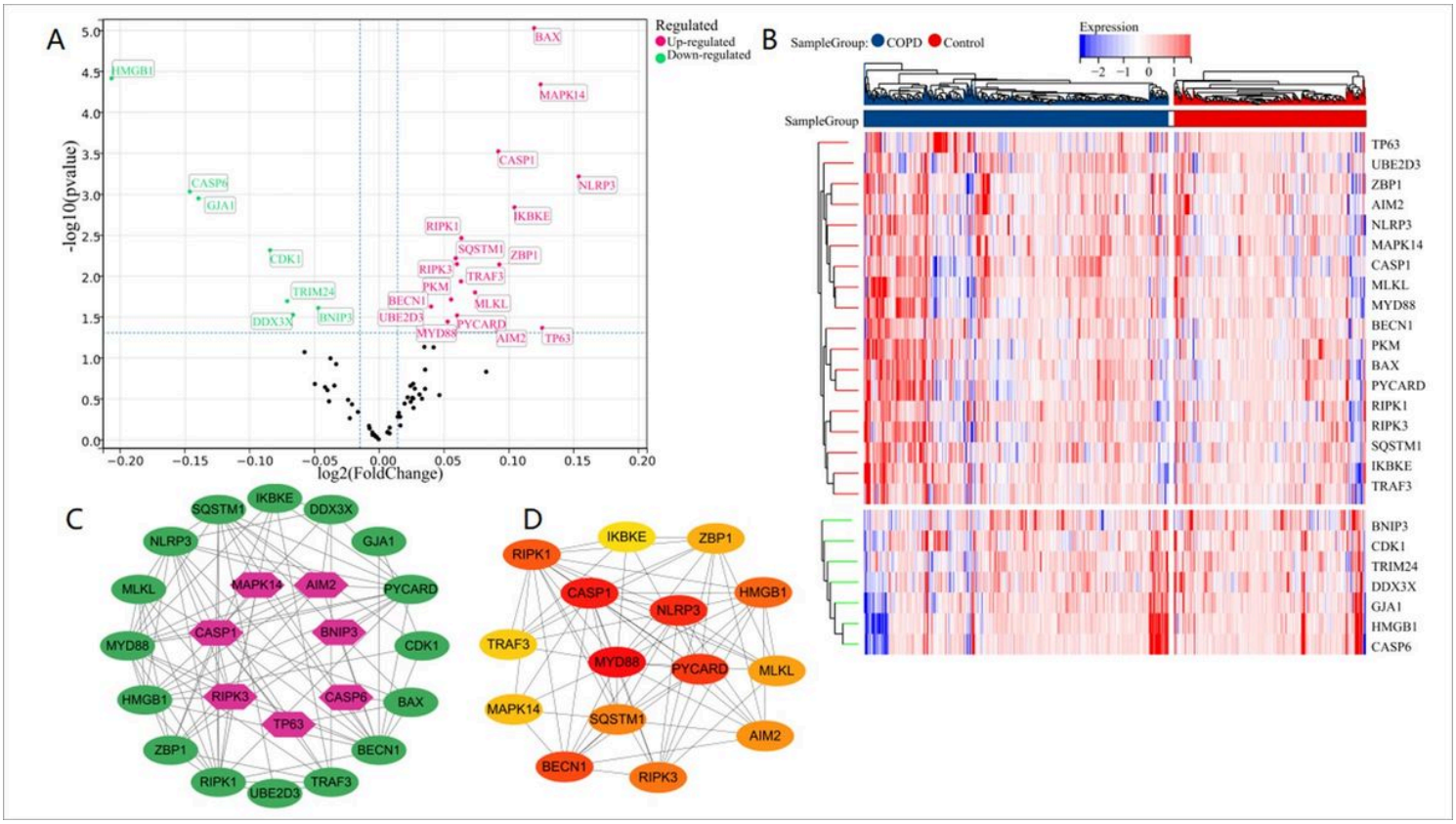

Figure 4

Exploring the 25 significant PANoptosis genes in COPD. A. The 25 significant DEGs identified among 71 PANoptosis genes in COPD were displayed in a volcano plot. Up-regulated genes are marked with red, and down-regulated genes are marked with green. **B.** Heatmap of the 25 significant DEGs. **C.** PPI network constructed via Cytoscape. Colors represent BC values from high (purple) to low (green). **D.** 15 hub clustering module based on BC values obtained from Cytoscape plug-in Cytohubba. Colors represent BC values from high (red) to low (yellow).

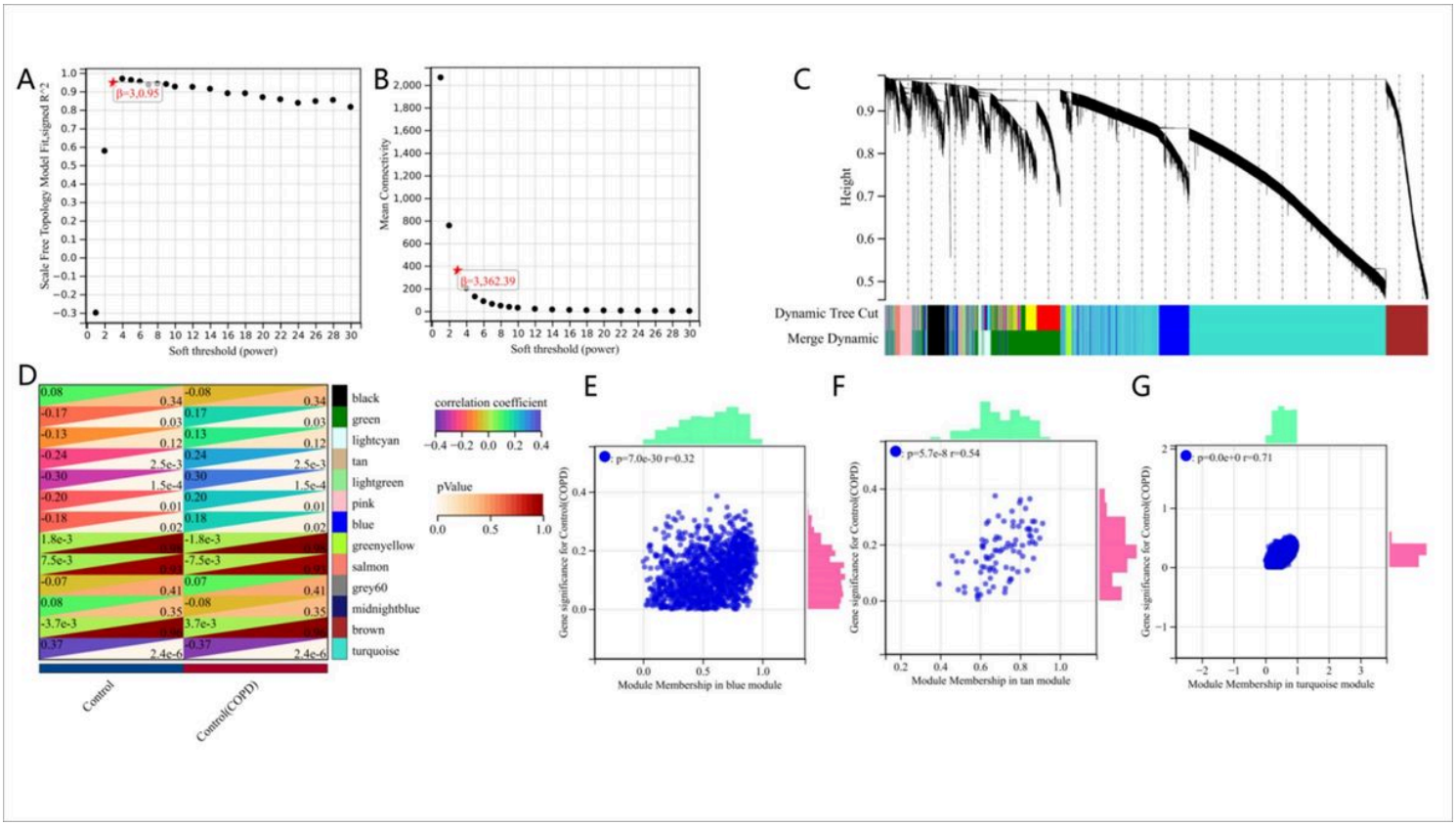

Figure 5

Validation of PANoptosis genes in COPD by WGCNA analysis. A-B. Determination of soft-thresholding power (β)in WGCNA. **A.** Analyzing scale-free fit index with β. **B.** Analyzing the mean connectivity with β. **C.** Clustering dendrogram shows module assignment based on β. **D.** The relationship between module features (MEs) and clinical traits using heatmap. Each row reflects an ME, and every column reflects the control or COPD group. **E-G.** The scatter plot indicates the significant genes in the blue module, tan module, and turquoise module.

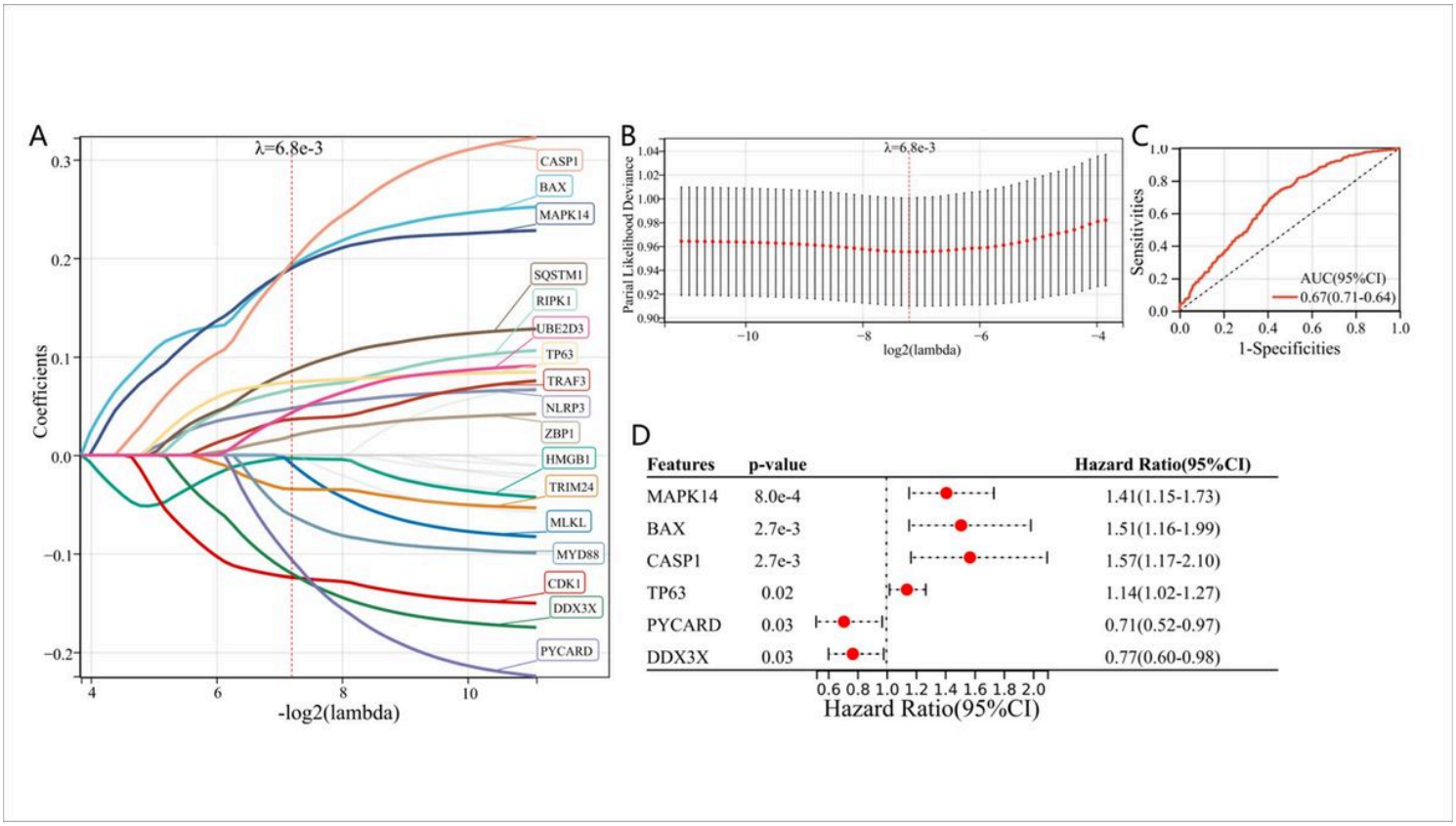

Figure 6

Construction and validation of risk signatures by LASSO-COX logistic regression algorithm. A-B. In the LASSO model, ten-fold cross-validation and optimal parameter (lambda)for hub gene coefficients. **C.** LASSO-COX logistic regression algorithm model was validated by risk score ROC curve. **D.** The optimized diagnostic markers were identified by survival analysis using COX method.

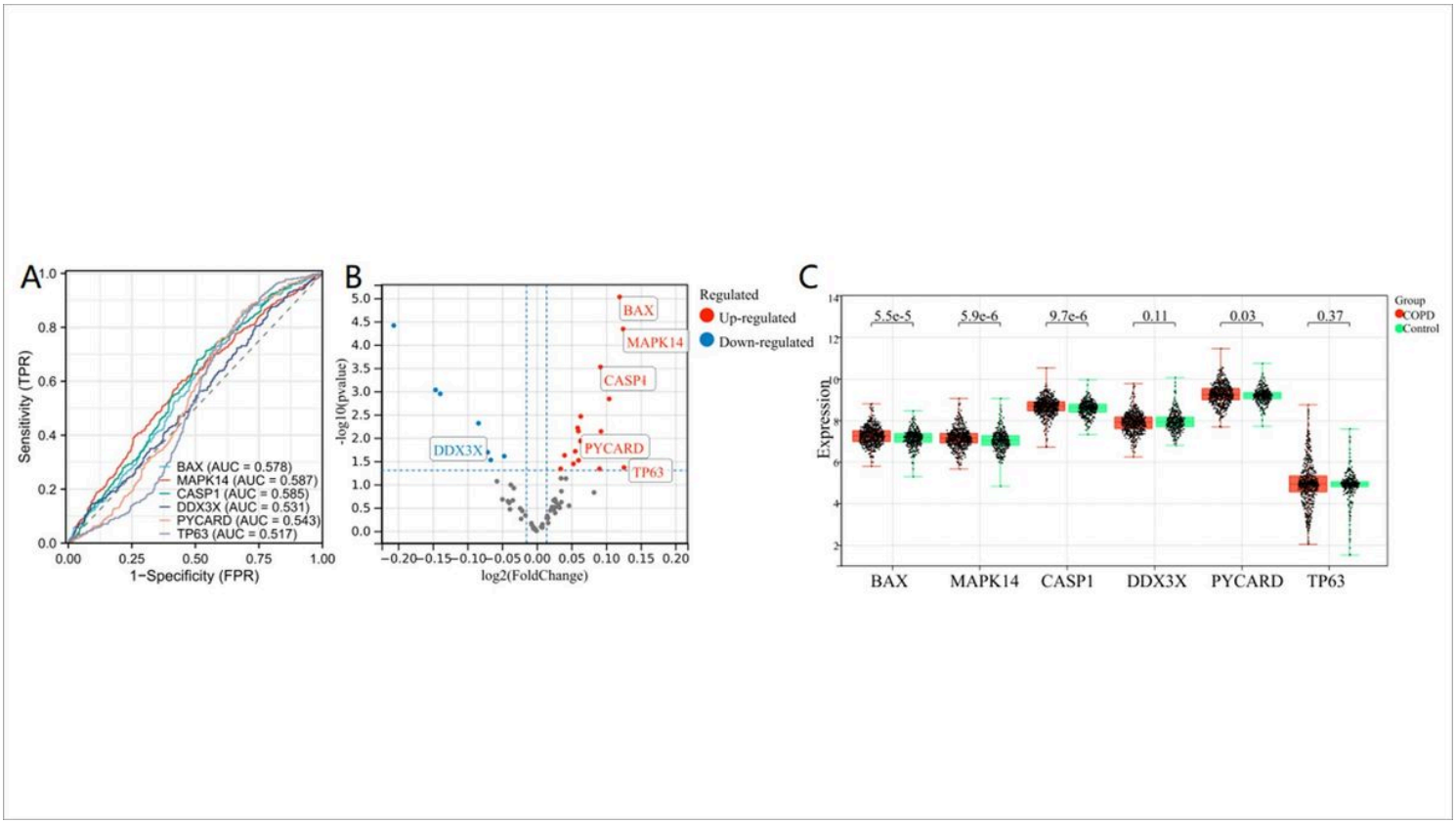

Figure 7

The screen of hub PANoptosis genes in COPD. A. Validation of BAX, MAPK14, CASP1, DDX3X, PYCARD, and TP63 by ROC curves in the merged COPD dataset which contained 5blood/lung datasets. **B.** Volcano diagram illustrates the expression of 6 genes in the merged COPD dataset. **C.** The expression of 6 hub PANoptosis genes COPD patients compared with normal samples.

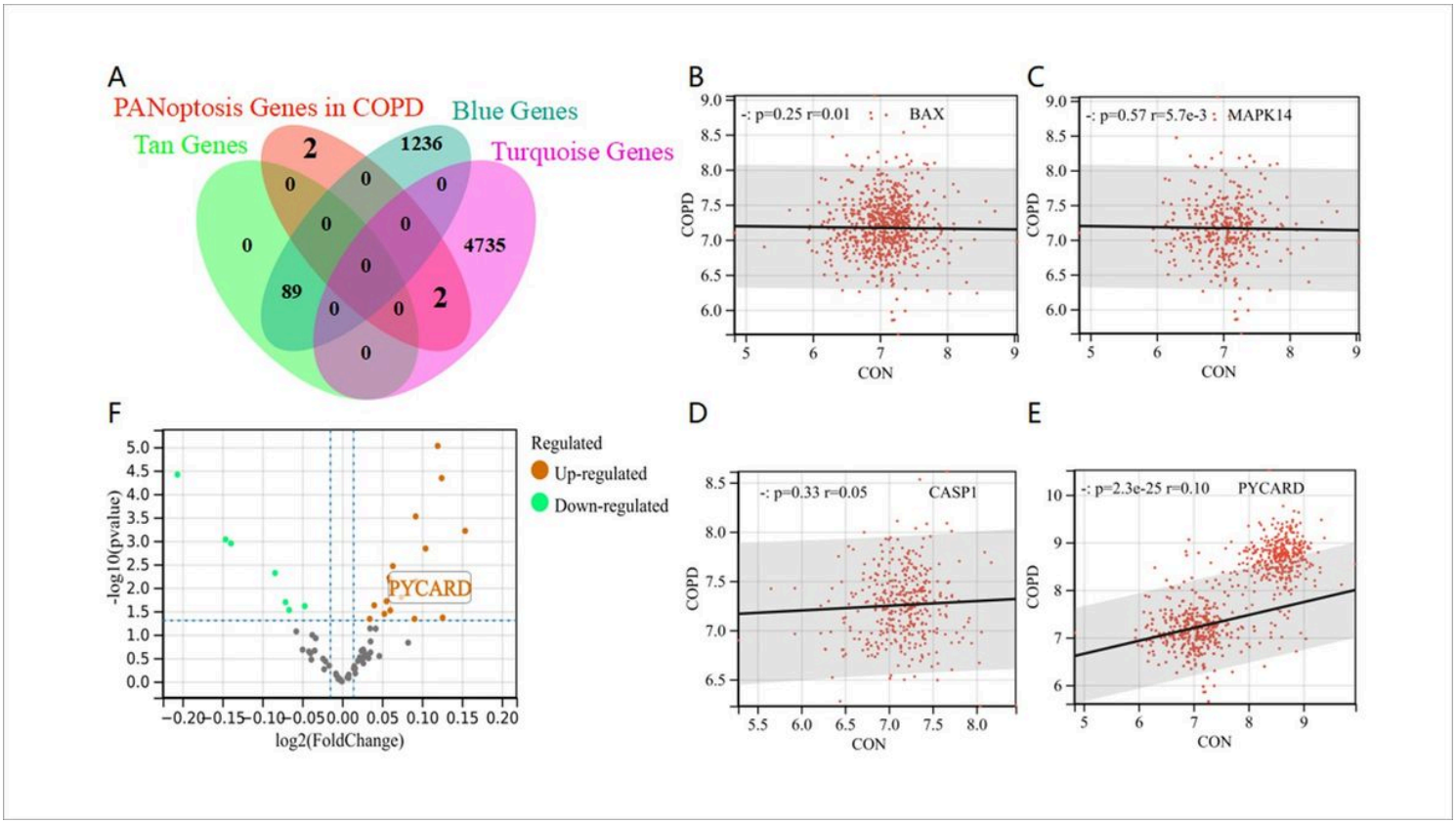

Figure 8

Identifying and validating PYCARD as a potential target for COPD. A. Venn diagram shows intersected 4 hub PANoptosis genes (BAX, MAPK14, CASP1, PYCARD) in COPD and the significant genes in blue module, tan module, and turquoise module. **B-E.** Scatter plot demonstrates the correlations of BAX, MAPK14, CASP1, PYCARD, and COPD patients with control samples. **F.** The expression of PYCARD is illustrated by a volcano plot. Upregulated genes and downregulated genes are shown in red (log2 (FC) > 0.99) and green, respectively (log2 (FC) < -0.99), $P < 0.05$.

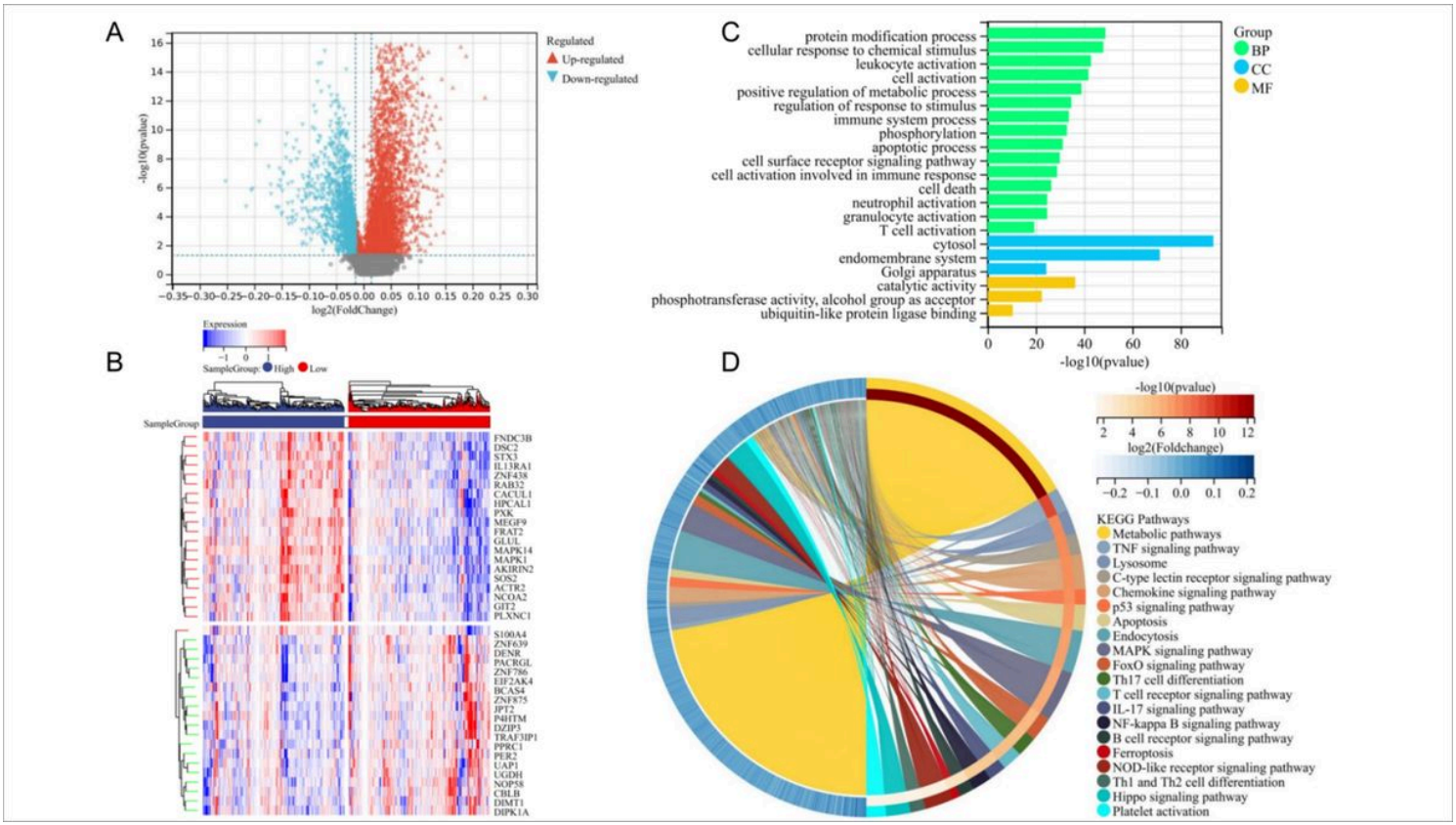

Figure 9

Differential and functional enrichment analysis of PYCARD grouping. **A.** Volcano graph is the differential analysis of PYCARD high and low expression groups in the merged COPD dataset. Red dots indicate the PYCARD high expression group and blue dots indicate the PYCARD low expression group. **B.** Heatmap demonstrates differential analysis for PYCARD expression. Red represents high expression, and blue represents low expression. **C-D.** GO and KEGG analysis for DEGs. **C.** Bargraph for DEGs in top 20 GO terms analysis. Each column corresponds to a term. the higher the column, the smaller *P*. Green column indicates BP, blue column indicates CC, yellow column indicates MF. The outer circle is the molecule in the entry, and the different heights represent the corresponding logFC value. **D.** Top 20 KEGG pathways among DEGs using loop diagram.

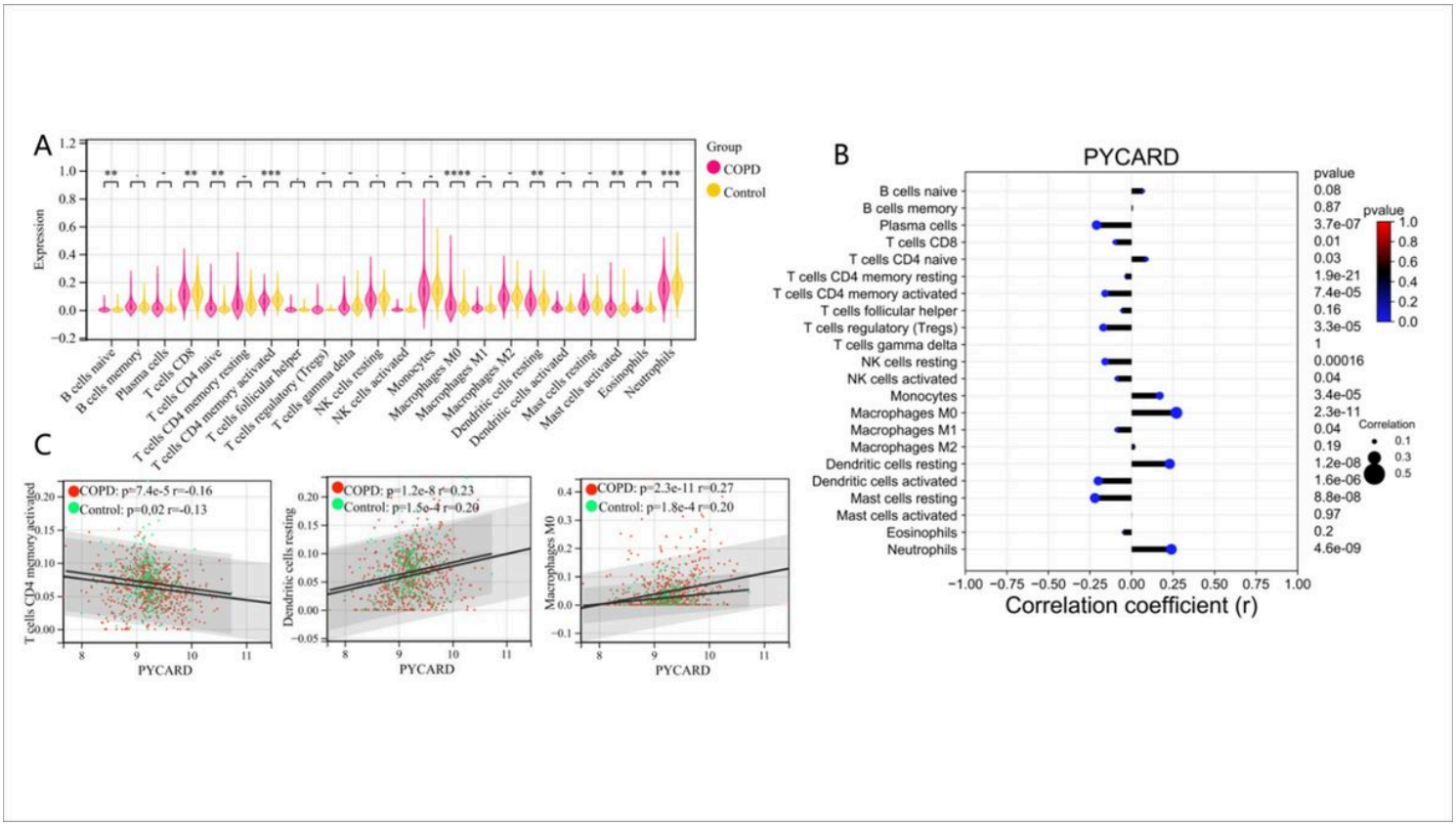

Figure 10

Immune cell infiltration and correlational analysis. A Voilin plot displays the proportion of 22 types of immune cells in the combined sepsis dataset. Pink is COPD samples, and yellow is normal samples. The significance infiltrated immune cells are shown as: -, $P > 0.05$; *, $P < 0.05$; **, $P < 0.01$; ***, $P<0.001$. **B** The lollipop graph of the correlation of PYCARD and infiltrated immune cells. The color of dots represents *P*-value, blue indicates a smaller *P*-value, and red indicates a higher *P*-value. A larger dot is a higher correlation. The left of the diagram labels a negative correlation, and the right part labels a positive correlation. **C.** Scatter plot of the correlation between PYCARD and 3-type differential immune infiltration cells.

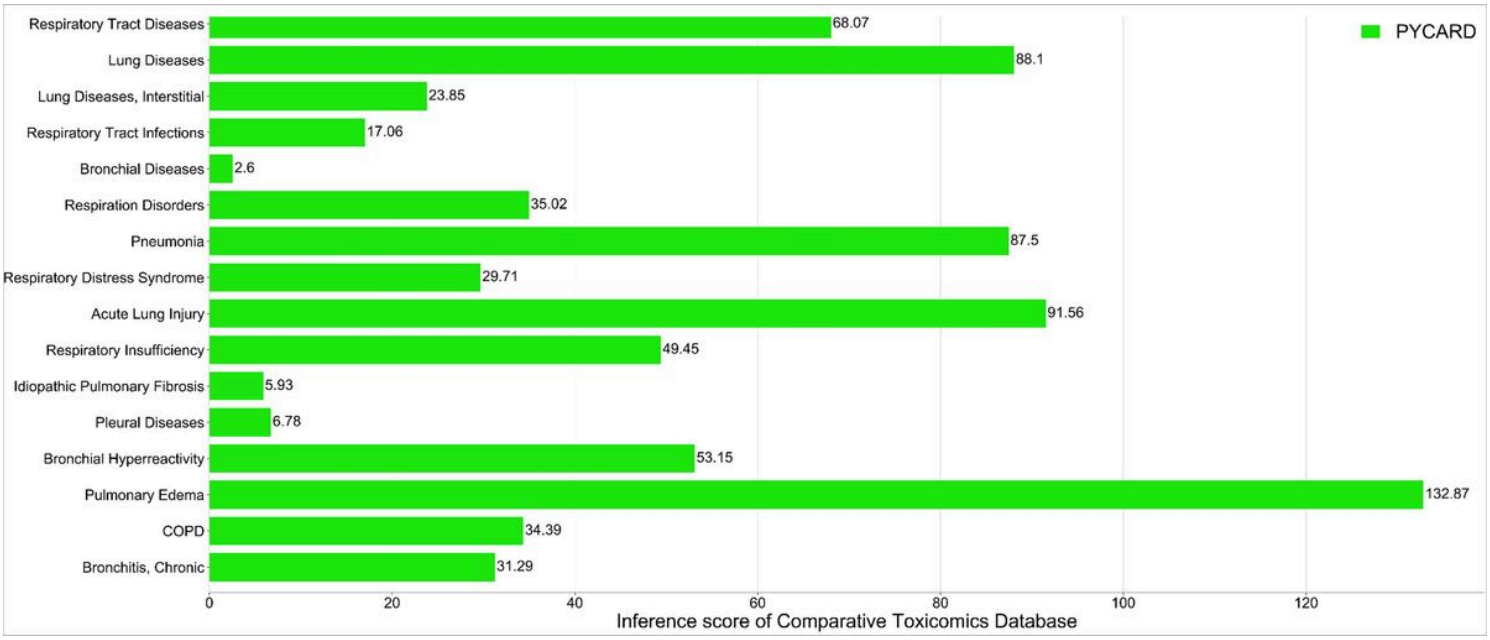

Figure 11

The analysis of correlations between PYCARD and respiratory tract diseases using the comparative toxicomics database.

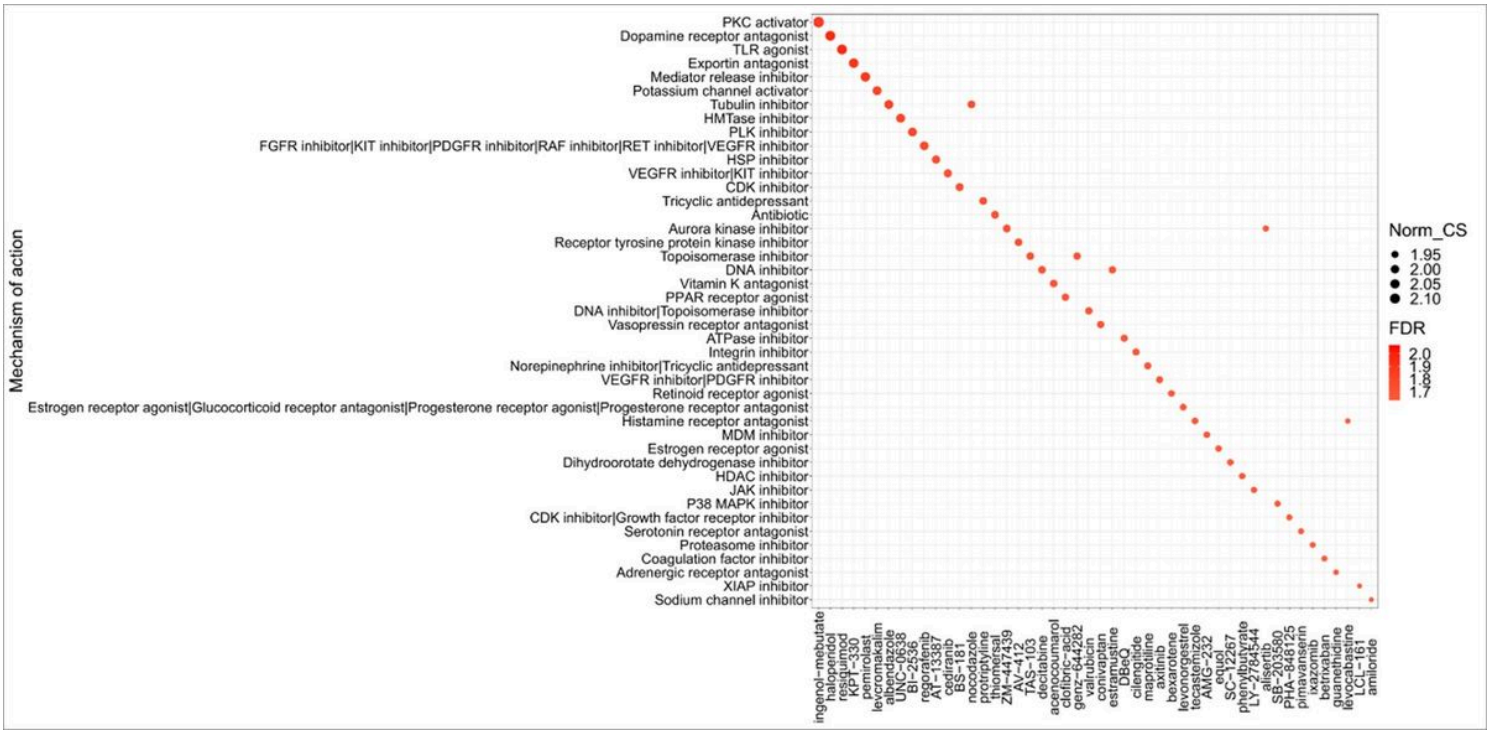

Figure 12

Identification of the molecular compounds with their mode of action in CMAP database.

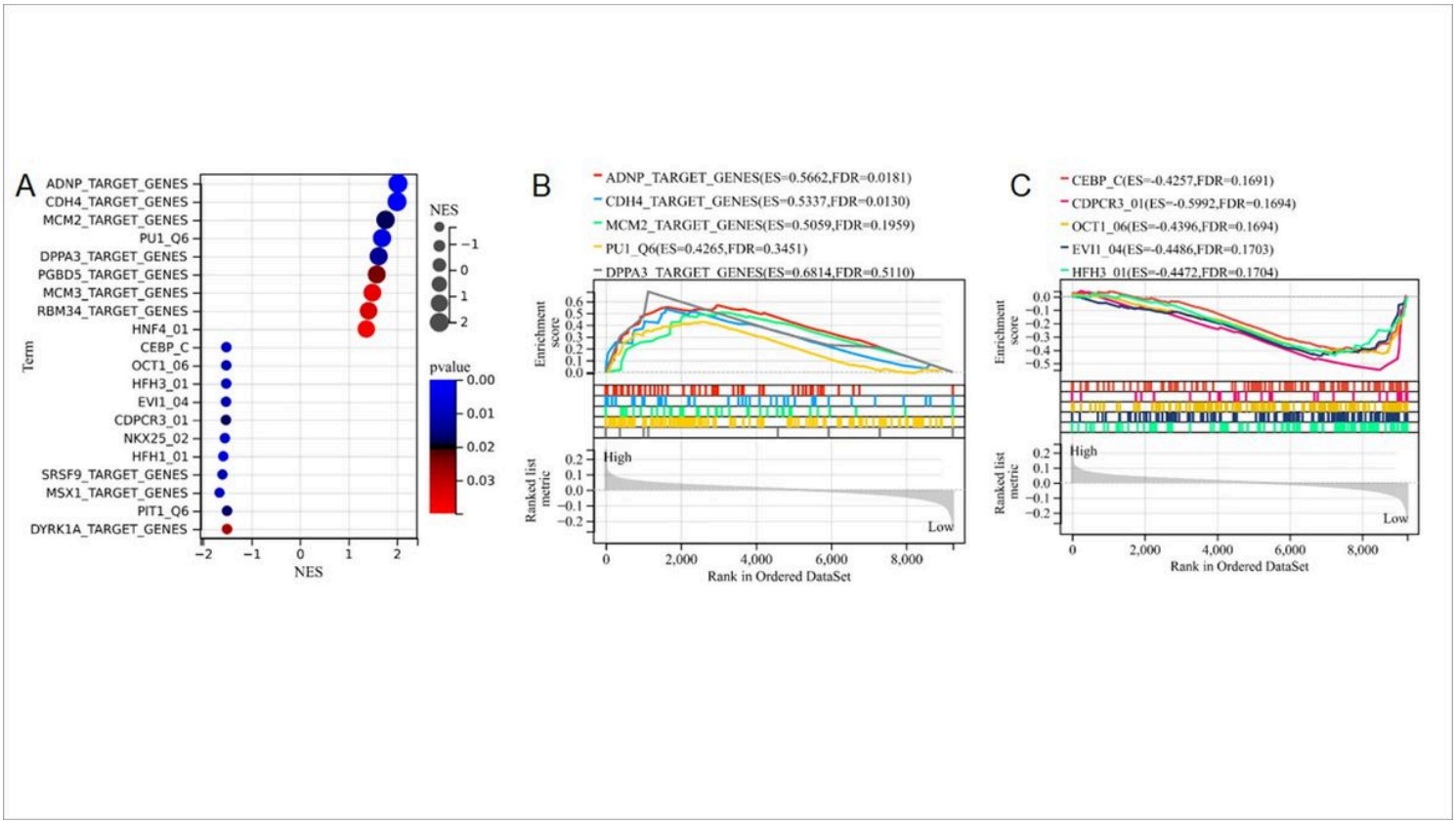

Figure 13

Screening and predicting the target genes of PYCARD. A.Target genes with up-regulated, and down-regulated by GSEA analysis. **B.** Top 5 positively related target genes of PYCARD. **C.** Top 5 negatively related target genes of PYCARD.

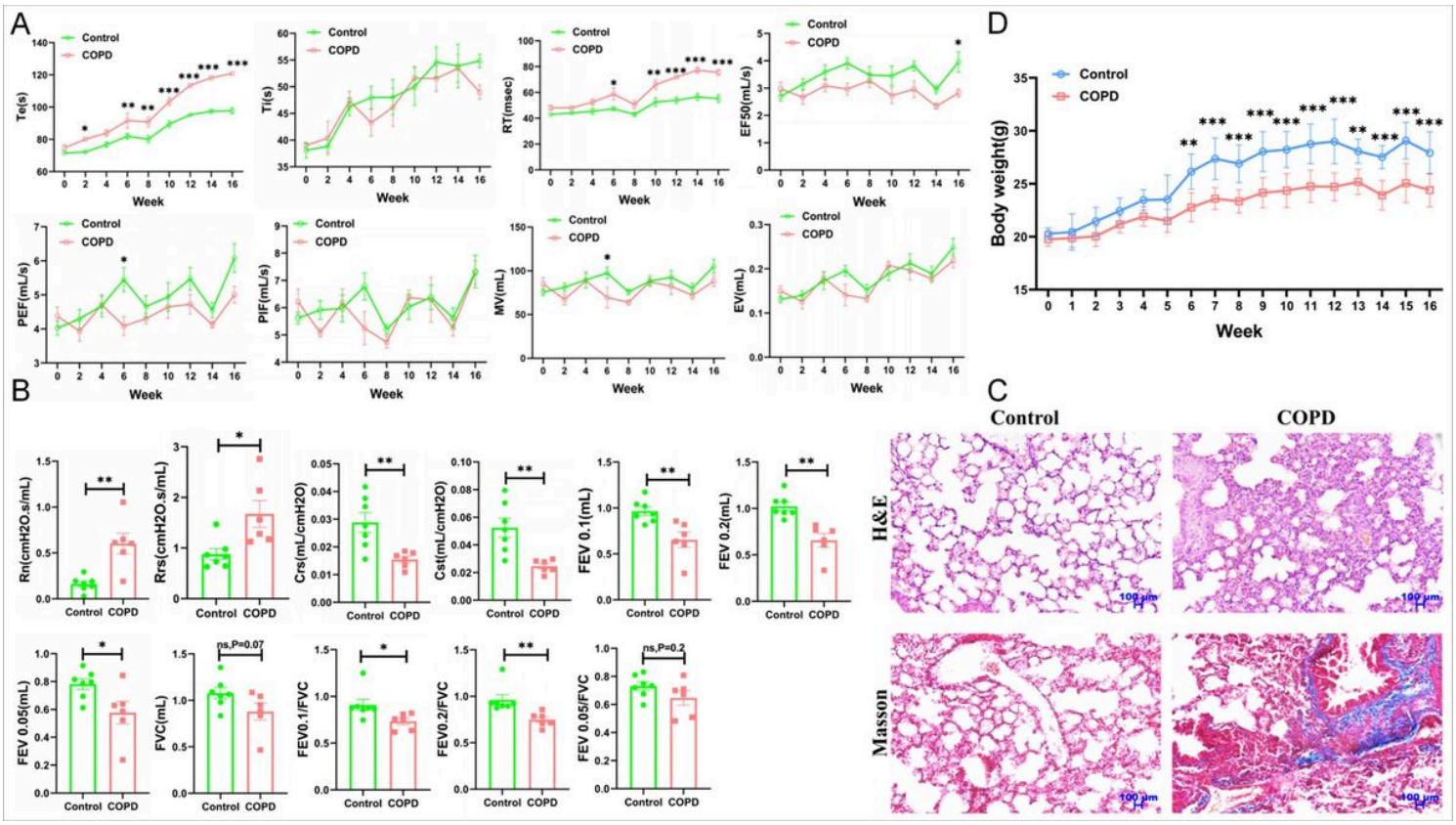

Figure 14

Pulmonary function and pathological damage of lung tissue in COPD model mice. A. Pulmonary function in conscious mice exposed to cigarette smoke from 0-16 weeks. Expiratory time (Te), inspiratory time (Ti), relaxation time (RT), expiratory flow at 50% tidal volume (EF50), peak expiratory flow (PEF), peak inspiratory flow (PIF), maximum minute ventilation (MV), expiratory volume (EV), n = 6-7. **B.** Invasive lung function in control group and COPD mice was measured at 16 weeks. Newtonian resistance (Rn), respiratory resistance (Rrs), compliance respiratory system (Crs), static ompliance (Cst), forced expiratory volume in 0.1 s (FEV0.1), forced expiratory volume in 0.2 s (FEV0.2), forced expiratory volume in 0.05 s (FEV0.05), forced vital capacity (FVC), forced expiratory volume in 0.1 s/forced vital capacity (FEV0.1/FVC), forced expiratory volume in 0.2 s/forced vital capacity (FEV0.2/FVC), and forced expiratory volume in 0.05 s/forced vital capacity (FEV0.05/FVC) in each group, n = 6-7. **C.** Representative images of H&E (Upper panel) and Masson (Lower panel) staining in control group and COPD mice (CS/LPS) lung tissue. Scale bar = 100 μm. **D**. Body weight in control and COPD model mice, n = 6-7.

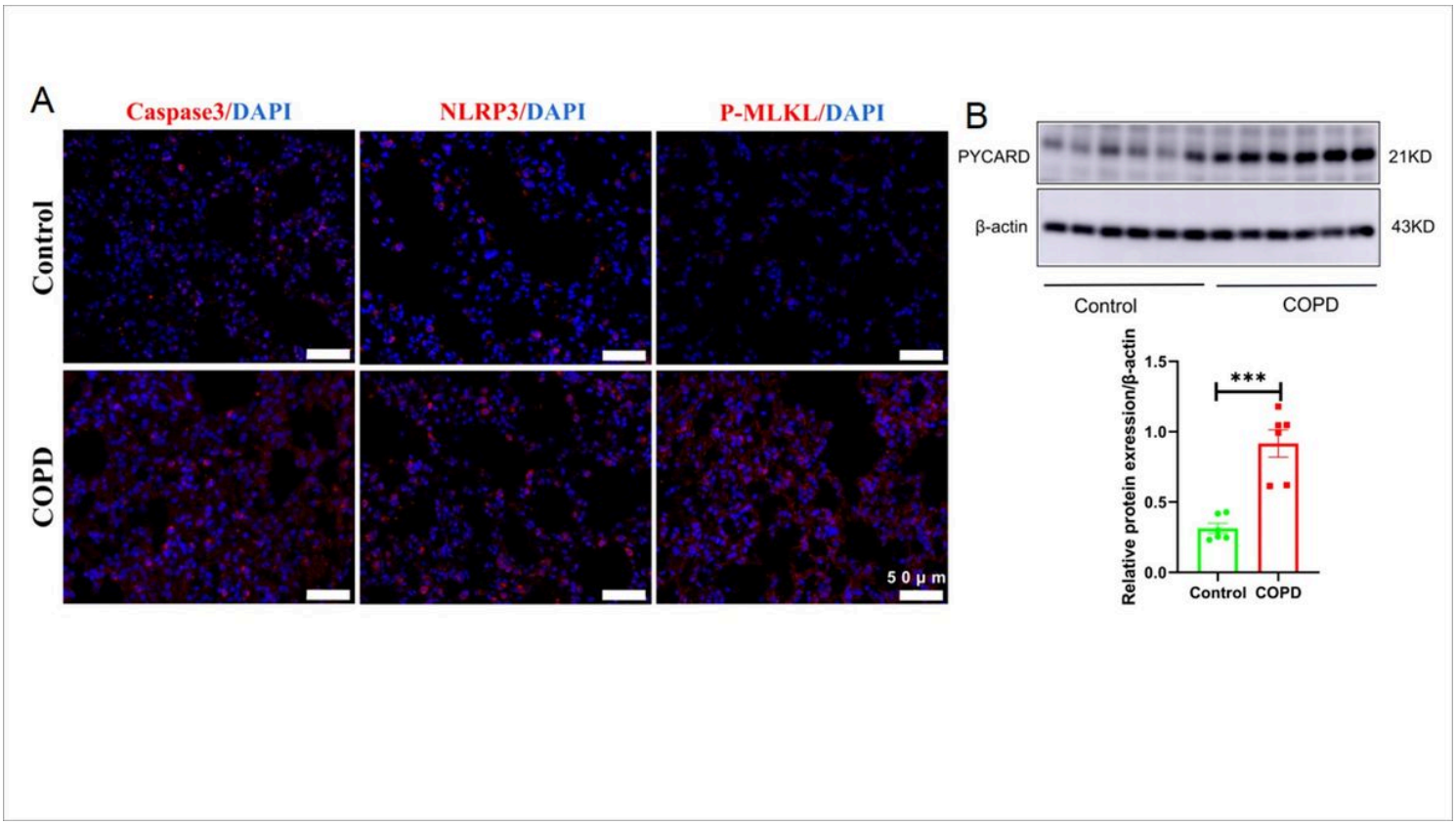

Figure 15

validating the target genes of PYCARD in COPD mice. A. Representative images of immunofluorescence staining of Caspase3, NLRP3, and p-MLKL (red) in lung tissue (Scale bar = 50 μm), n = 3. **B**. PYCARD protein levels in the lung tissues of each group were detected by Western blot, n = 6.

Supplementary Files

This is a list of supplementary files associated with this preprint. Click to download.

- SupplementarydataApoptosis.docx